SHIELDING CALCULATIONS FOR A TANK-IN-POOL REACTOR

BY

JOSEPH K. GBADAGO

A DISSERTATION PRESENTED TO THE UNIVERSITY OF GHANA, LEGON FOR THE AWARD OF THE MASTER OF PHILOSOPHY (M.PHIL. PHYSICS) DEGREE

JULY, 2000.

TABLE OF CONTENTS

DEDICATION

I dedicate this work to my father Mr. Augustine Kodjo Sabbor Gbadago of blessed memory and to my mother Theodora Kudowor-Gbadago for the sacrifices they made in laying the foundation of my education.

DECLARATION

I declare that, except for references to other people's work, this thesis is the result of my own research and that it has neither in part nor whole been presented elsewhere for another degree.

.....

JOSEPH K. GBADAGO

(STUDENT)

DATE.....July 10, 2000.....

.....

PROF. G.K. TETTEH

(SUPERVISOR)

DATE.....17/7/2000.....

.....

PROF. E.H.K.AKAHO

(CO-SUPERVISOR)

DATE.....13TH JULY 2000.....

ACKNOWLEDGEMENT

I wish to express my most heartfelt thanks to my supervisors, Professor G.K. Tetteh of the Department of Physics, University of Ghana and Professor E.H.K. Akaho of the Department of Nuclear Engineering, Ghana Atomic Energy Commission (G.A.E.C.) for their useful guidance and criticism.

My gratitude also goes to Dr. Shiloh Osae and Messrs. Samuel Anim-Sampong, B.T. Maakuu and Edison Amanor, all of the Ghana Research Reactor-1 Centre (GHARR-1C) of G.A.E.C. for their immense assistance. My special thanks also go to Mr. Allison Hughes a course mate, Mr. Daniel Ahiatsi-Mensa and Miss Rosemond Amonoo, colleague students of the University of Ghana, for their love and encouragement.

I wish to register my sincere appreciation to the Management Board of G.A.E.C. for permitting the use of its facilities.

My sincere thanks go to my parents and siblings for their love and care, and to all those who in diverse ways contributed to my education.

Finally, I thank God the Almighty Father for seeing me through another Chapter of my education. To Jesus be the glory!

ABSTRACT

The effectiveness of the water shield above the core and in the pool for shielding gamma rays and neutrons was investigated by measurements and calculations for a tank-in-pool type reactor, Ghana Research Reactor-1, GHARR-1. Experimental determination of γ – dose rates were made using Radiation Alert Monitor-4 and halogen counter type J613 γ probe with readout on γ -radiation monitoring system of the control console and the microcomputer control system. The PC version of the one-dimensional transport code ANISN was used to estimate the gamma and the neutron dose-rates at various positions of the reactor. All computations were carried out using the S_8 angular quadrature in a cylindrical geometry pertaining to the reactor GHARR-1. The P_3 scattering order was assumed. The microscopic cross-sections of materials for various regions were extracted from VITAMIN C master library consisting of 171 neutron and 36 photon energies. Concentrations in various regions were computed based on procedures outlined in WIMS-D/4. The calculational result of gamma dose rate was 25.8 $\mu Sv / hr$ at the edge of the pool for nominal power of 30kW which agreed with the experimental one of 25 $\mu Sv / hr$. The maximum and minimum percentage variation of the calculational and the experimental results were 8.21 and 0.27 respectively with corresponding standard deviations of 0.42 and 0.04. Based on this satisfactory result, the dose profile along the slant tubes used to commission the reactor was studied using the code and an assessment was also performed for the radiological consequences of postulated accidents due to loss-of-coolant accidents. With the available information on the variation of the neutron and the gamma doses along the slant tubes, high dose thermolumniscent (TLD) badges could be used to confirm the calculated values in the future. The tubes could then be mapped for studies on the effect of neutron and gamma irradiation on mutation breeding of seeds in the field of agriculture. The effectiveness of the shielding in the case of loss-of-coolant due to a break in the pipe of the reactor vessel or crack in the pool caused by an earthquake was investigated. The results of the study indicate that the dose rates around the reactor vessel and pool would be abnormally high. However, core melt-down is not expected because the design features of the reactor are such that the core will remain covered with coolant in the event of a break in a pipe line to the purification plant.

CHAPTER 1

INTRODUCTION

The main purposes of a reactor shield system are to protect operating personnel from possible injury by escaping radiation and in some cases to reduce the radiation exposure of structural components. Since the radiations entering the shield from the reactor can produce internal heating and possibly cause radiation damage to shield materials, it is necessary to estimate the types and intensities of the radiations throughout the shield. The shielding of nuclear reactor systems is therefore concerned with the study of radiation distribution in the shield, for the dual purpose of reducing the escaping radiation to acceptable levels and of limiting the adverse physical effects on the shield materials [1,2]. In principle, the radiations which might escape from a reactor system include alpha and beta particles, gamma rays, neutrons of various energies, fission fragments, and even protons resulting from (n, p) reactions. As far as shield design is concerned, however, only gamma rays and neutrons need be considered since these are by far the most penetrating. Any material which attenuates these radiations to a sufficient extent will automatically reduce all the others to negligible proportions [3].

Some indication of the complex character of the nuclear radiations due to neutrons and various gamma radiations arising from a reactor is apparent from Fig.1.1. The fission process itself produces fission fragments, neutrons, and gamma rays. These undergo various reactions both within the reactor itself and in the shield, leading to the formation of a complex variety of other radiations. For the purpose of shield design, the neutrons and gamma rays are considered from the standpoint of their place of origin: the primary radiations are defined here as those which originate within the core, whereas the secondary radiations are produced outside the core as a result of the interaction of the primary radiations, chiefly the neutrons, with nuclei in the reflector, coolant, and shield materials [3].

The most significant primary radiations are fast neutrons, the prompt fission gamma rays, the decay gamma rays from fission products, and capture gamma rays. There are also thermal neutrons, inelastic scattering gamma rays, and decay gamma rays from radioactive products of neutron capture reactions. The gamma rays in this latter group are of very low energy and therefore non-penetrating consequently, they do not significantly affect the shield thickness, but the neutrons captured outside the core produce secondary gamma rays which are very important [4,5].

In considering the applicability of a particular calculation procedure, it is advantageous to have a knowledge of the major sources of error that in general affect calculations in the particular field of study. Uncertainties in source data, and basic cross section data contribute to errors in estimating shield thickness. In addition, inadequacies of the calculational methods and complexity of geometries may lead to errors. It is generally accepted that in most practical shielding calculations, the main single source of error stems from the simplifications that must be made concerning the complicated geometry.

When first considering the subject of shield analysis, it may appear that there is little need to distinguish between shielding calculations procedures and reactor calculation procedures, since the

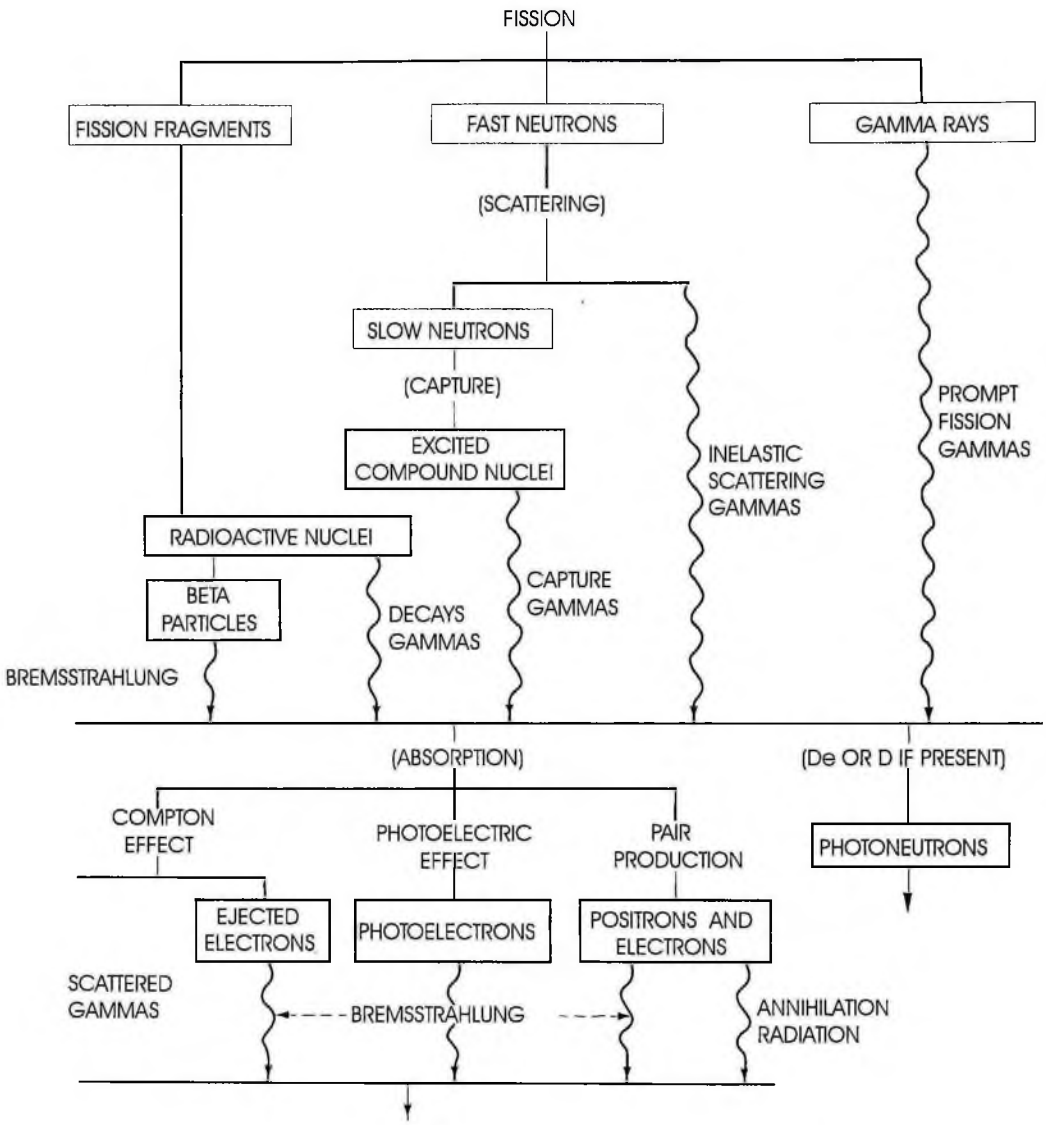

Fig. 1.1. Radiations from a nuclear reactor.

behaviour of the particles of interest in both fields can be described by the same Boltzmann transport equation. But there are special features of the typical shielding problem which have led to the development of techniques peculiar to shield analysis. The distinctive features of the shield problem can be summarized as;
(a) the distribution of the source of radiation is not restricted to the reactor core; the source is also distributed throughout the shield;
(b) the severe reduction in the radiation intensity during transit of the shield [6].

The Ghana Research Reactor-1 (GHARR-1) is a commercial Miniature Neutron Source Reactor (MNSR),installed at the National Nuclear Research Institute (NNRI) of the Ghana Atomic Energy Commission (GAEC) in Kwabenya. Detailed description of the reactor is presented in Chapter 4.

For shielding of neutron and gamma-rays, the reactor vessel and the pool are filled with deionized water to certain levels. The levels are monitored on the control console and the reduction in levels would lead to high gamma doses which would be detected on the monitoring system of the control console or the microcomputer control system. However, there is the need to ascertain the effectiveness of the water shield above the core.

In the Safety Analysis Report (SAR) for the Ghana Research Reactor-1 [7] , the postulated accident of Loss - of - Coolant Accident (LOCA) for the reactor vessel and pool were discussed. Actual calculations of dose rates were not performed to ascertain the effectiveness of the water shields. There is the need therefore, to simulate the postulate. In addition, two slant tubes are attached to the lower section of the reactor vessel in the region of the core. The tubes were used for commissioning. After the commissioning, the slant tubes form part of the reactor. It is envisaged that the tubes can be used to study the effect of neutron and gamma irradiation on mutation breeding of seeds. There is therefore the need to determine the variation of dose rates around and along the tubes. The objective of this thesis is therefore three- fold:

(1) Theoretical shielding calculations of dose rates using one-dimensional (1-D) transport code ANISN for neutron- and gamma-dose rates for different power levels at different positions around the pool and the reactor vessel, and the experimental measurement of dose rates using Radiation Alert Monitor-4 and Halogen Counter Type J613 γ GM probe instruments. The experimental results will be used to validate the computational results by the ANISN code for the GHARR-1. Based on the validation, the ANISN code will be used to;

(2) Determine the variation of dose rates with distance along and around the slant tubes, for possible mapping of dose rates in the future for the study on the effect of neutron and gamma irradiation on mutation breeding of seeds in the field of agriculture.

(3) Simulate postulated accidents of loss-of-coolant in reactor vessel and pool.

In Chapter 2, the computational methods are reviewed. Chapter 3 describes the application of 1-D transport code ANISN to GHARR-1 reactor shield analysis.

Chapter 4 presents the neutron and the gamma dose rates for normal operational conditions. Chapter 5 presents the estimation of neutron and gamma dose rates for loss-of-coolant accidents, and finally the main conclusions and recommendations for future works on GHARR-1 are presented in Chapter 6.

CHAPTER 2

COMPUTATIONAL METHODS

In shielding calculations, analytical and computational methods are widely used. The analytical method is useful primarily to provide background for the principles involved as well as to provide estimates of neutron and gamma-ray attenuation in shields for preliminary designs. However, for design purposes, more exact computer methods are necessary. Although the use of computer methods is required for all phases of nuclear design, it is particularly true for shield applications for two reasons. First, the directional aspect of radiation transport through the various layers of a shield system requires the applications of the Boltzmann transport equation. Secondly, acceptable exposure levels outside the shield demand attenuation of the neutron and gamma-ray levels by many orders of magnitude with little margin for error. Thus the power of sophisticated codes are preferred to analytical methods [3,8].

The use of a particular code in a reactor shield analysis depends on the geometry in question. For instance, the discrete ordinates technique for obtaining approximate solutions to the transport equation, is commonly used for 1-D shielding calculations, for example, by the ANISN code [9]. Codes such as the DOT-111 [10] are used for 2-D calculations. For relatively simple geometries, use of Monte Carlo codes such as MORSE [11] and KENO V.a [12] are usually neither justifiable nor necessary. However, for more complex shield geometries, where a 3-D treatment is required, the Monte Carlo method is preferred. In some cases, the overall analysis may be simplified by using the discrete ordinate method in part of the calculation and the Monte Carlo method in another part. Other combinations of procedures for solving the transport problem are also possible[11,13,14].

2.1. THE TRANSPORT EQUATION

Although the linear Boltzmann equation can be derived from first principles of physics, it is more easily obtained by a simple balancing of the various mechanisms by which particles can be gained or lost from an element in a phase-space (r, Ω, E), that is

Time rate of particle density change	=	Change due to Physical leakages	+	Change due to collisions	+	Sources.

This balance condition may be expressed mathematically as

$$\frac{1}{v}\frac{\partial\Phi(\mathbf{r},\Omega,E,t)}{\partial t} = -\Omega.\nabla\Phi(\mathbf{r},\Omega,E,t) - \sum_t(\mathbf{r},E,t)\Phi(\mathbf{r},\Omega,E,t) + \int_0^\infty dE' \int_{4\pi} d\Omega' \sum(\mathbf{r};E' \to E;\Omega'.\Omega,t)\Phi(\mathbf{r},\Omega,E',t) + S(\mathbf{r},\Omega,E,t). \quad (1)$$

where

r is the position of the particle at a time t

Ω is the direction in which the particle moves

E is the energy of the particle

v is the speed of the particle

$\Phi(\mathbf{r},\Omega,E,t)$ is the angular flux, or angular particle path length

$\sum_t(\mathbf{r},E,t)$ is the total macroscopic cross section.

$\sum(\mathbf{r},E' \to E,\Omega'.\Omega;t)$ is the differential transfer cross section.

$S(\mathbf{r},\Omega,E,t)$ is the source term.

The first term is the rate of change of particle density .
The second term represents the change due to physical leakages.
The third term is the change due to collision due to absorption.
The fourth term is the change in energy and direction at time t due to collision scattering process (ie the transfer kernel term).
The last term accounts for group fixed sources.

Eqn.(1) can be applied to neutrons or photons, depending on the correct physical interpretation of the interaction between the particle and the host medium.

For neutrons, besides a scattering reaction, a collision of neutrons with a host medium can generate other neutrons by fission (multiplying medium) and so the transfer kernel may include a term like

$$\frac{\chi(E)}{4\pi}\int_0^{\infty} dE' \int_{4\pi} d\Omega' \nu(E') \sum_f (\mathbf{r}, E', t)\Phi(\mathbf{r}, E', \Omega', t) \tag{2}$$

where

$\chi(E)$ is the energy distribution of fission neutrons .

$\nu(E')$ is the average number of neutrons released per fission and

$\sum_f (\mathbf{r}, E', t)$ is the macroscopic fission cross section, assumed to be isotropic.

Usually, for practical applications, Eqn.(1) is solved in steady-state. Also, in case of multiplying media, it is to be expected that systems containing fissile nuclides can be regarded as being either subcritical, critical, or supercritical. The criticality problem can often be best approached by introducing the effective multiplication factor , K_{eff} , to balance the fission source with other terms in the transport equation, in a manner such that the resulting system is critical, that is, any system containing fissile material could be made critical by varying the number of neutrons emitted per fission from the original value (ν) to, (ν/k). Therefore, Eqn.(1) is rewritten in the form

$$\begin{aligned}&\Omega.\nabla\Phi(\mathbf{r},\Omega,E,t)+\sum(\mathbf{r},E,t)\Phi(\mathbf{r},\Omega,E,t)=\\&\int_0^{\infty}\int_{4\pi}\sum_S(\mathbf{r},\Omega'\to\Omega,E'\to E)\Phi(\mathbf{r},\Omega',E')d\Omega'dE'\\&+\frac{1}{K_{eff}}\int_0^{\infty}\int_{4\pi}\frac{\chi(E)}{4\pi}\nu(E')\sum_f(\mathbf{r},E')\Phi(\mathbf{r},E',\Omega')d\Omega'dE'+S(\mathbf{r},E,\Omega,t)\end{aligned} \tag{3}$$

The scattering kernel depends on the physical interaction, and usually, the angular dependence is expanded in Legendre polynomials (P_l) of the scattering angle ($\Omega.\Omega' = \mu_0$); that is,

$$\sum_s(\mathbf{r},E'\to E,\mu_0)=\sum_{l=0}^{L}\frac{2l+1}{2}\sum_s^{(l)}(\mathbf{r},E'\to E)P_l(\mu_0) \tag{4}$$

The energy dependence is treated by a multigroup model, in which the energy range is divided into a finite number G, of intervals separated by the energies E_g ,g=1,2,3,...,G [15]. Thus the multigroup transport equation with anisotropic scattering, is written as;

$$\Omega.\nabla\Phi_g(\mathbf{r},\Omega)+\sum_{tg}\Phi_g(\mathbf{r},\Omega)=\sum_{l=0}^{L}\sum_{g=1}^{G}\int_{4\pi}d\Omega'(\frac{2l+1}{2})\sum_{g'\to g}(\mathbf{r})P_l(\mu_0)\Phi_g(\mathbf{r},\Omega')$$
$$+\frac{\chi_g}{K_{eff}}\sum_{g'}(\frac{\nu\sum_f}{4\pi})_{g'}\Phi_{g'}(\mathbf{r})+S_g(\mathbf{r}). \quad (5)$$

g=1,2,3,...G.

where

$\Phi_g(\mathbf{r},\Omega)$ is the angular flux and is given by

$$\Phi_g(\mathbf{r},\Omega)=\int_{E_g}^{E_{g+1}}\Phi(\mathbf{r},E,\Omega)dE; \quad (6)$$

and

$$\Phi_g(\mathbf{r})=\int_{\Omega}\Phi_g(\mathbf{r},\Omega)d\Omega$$

is the total flux [6].

The group cross sections, or group constants, $(\sum_{tg};\sum_{g'\to g}^{(l)};\chi_g;(\nu\sum_f)_g)$ are flux weighted cross sections averaged over the group energy interval, that is,

$$\sum_g(\mathbf{r})=\frac{\int_g\sum(\mathbf{r},E)\Phi(\mathbf{r},E)dE}{\Phi_g(\mathbf{r})} \quad (7)$$

and

$$\sum_{g' \to g}^{(l)}(\mathbf{r}) = \frac{\int_{g} dE \int_{g'} \sum^{(l)}(\mathbf{r}, E' \to E) \int_{4\pi} \Phi(\mathbf{r}, E', \Omega') P_l(\mu_0) dE' d\Omega'}{\int_{g'} \int_{4\pi} \Phi(\mathbf{r}, E', \Omega') P_l(\mu_0) dE' d\Omega'} \qquad (8)$$

The reason is that the group constants that appear in these equations depend on the knowledge of the group fluxes which are not known before solving the transport equation for the problem. To overcome this difficulty, it is used as weighting function $\Phi(\mathbf{r}, E)$ in Eqn. (7). The pointwise cross sections needed to evaluate the group cross section is given from Nuclear data libraries such as "Evaluated Nuclear Data File" (ENDF) [6].

Depending on the geometry of the radiation source, Eqn.(5) is transformed and solved numerically through computational procedures.

CHAPTER 3

APPLICATION OF 1-D TRANSPORT CODE ANISN FOR GHARR-1 SHIELD ANALYSIS

The 1-D transport code ANISN with its solution technique, the discrete ordinates method, is applied in this work.

In the next section, the numerical techniques employed by the code are reviewed.

3.1 NUMERICAL TECHNIQUES

ANISN is a 1-D transport code which forms part of an MTR_PC computer package. It was originally developed by Oak Ridge computing Technology Center and Oak Ridge National Laboratory[9], to solve the 1-D linear particle transport equation, also known as the linear Boltzmann transport equation numerically in plane, spherical or cylindrical geometry to estimate the particle flux[9,16]. The solution technique is an advanced discrete ordinates method which comprises a number of numerical techniques which have mostly been developed in the context of reactor calculations.

Since the GHARR-1 reactor is of cylindrical geometry, the streaming term($\Omega.\nabla\Phi_g$)of Eqn.(5) has to be expressed accordingly to pave the way for its numerical solution by the discrete ordinates technique employed by the ANISN code. The form of linear transport equation for Eqn.(5) in 1-D cylindrical geometry (r,μ,χ) becomes

$$\sqrt{1-\mu^2}\cos\chi\frac{\partial\Phi_g(r,\mu,\chi)}{\partial r}-\frac{\sqrt{1-\mu^2}}{r}\sin\chi\frac{\partial\Phi_g(r,\mu,\chi)}{\partial\chi}+\sum_{tg}\Phi_g(r,\mu,\chi)$$

$$=\sum_{l=0}^{L}\frac{2l+1}{4\pi}\sum_s^{(l)}(r)P_l(\mu)\int_{-1}^{1}d\mu'\int_0^{2\pi}d\chi\Phi_g(r,\mu',\chi')P_l(\mu')d\mu'+S_g(r,\mu,\chi) \qquad (9)$$

where l is the scattering order and $l=0$ for isotropic scattering.

For radiation shielding problem for gamma coupled systems the fission term in Eqn.(2) used for criticality search is not included in Eqn.(9).

There can be further simplification of equation (9). In order to couple neutrons and gammas, the equation is divided into sets, an upper set consisting of N-groups of neutrons (g=1,2,...,N) and a lower set consisting of G-groups of gammas (g=N+1, N+2,...,N+G).the two sets are coupled by a transfer cross section ($\sum_{n\to g}$) due to nuclear cross sections with neutrons producing gammas, that is, capture or inelastic scattering reactions [6,17].

The steady-state linear transport equation presented above applies to physical problems which are typical boundary value problems. There are different boundary conditions but the reflection boundary condition which is commonly used is applied in this study. This boundary condition assumes that particles are reflected at the surface with angle of incidence equal to the angle of reflection. Mathematically, it is expressed as

$$\Phi(\vec{r}_s,\hat{\Omega},E) = \Phi(\vec{r}_s,\hat{\Omega}^*,E), \qquad \hat{\Omega}.\hat{n} < 0 \qquad (10)$$

where

$$\hat{\Omega}^*.\vec{n} = -\hat{\Omega}.\vec{n}; \qquad \hat{\Omega}\times\hat{\Omega}.\vec{n} = 0 \quad ,n \text{ is a unit vector [6].}$$

Equation (9) is solved numerically by the discrete ordinates technique in the next section.

3.1.1. The Discrete Ordinate (S_N) Method.

An alternative to expressing the spatial distribution of the neutron angular flux Φ in terms of Legendre Polynomials is to employ the method of discrete ordinates [18]. In this procedure, the angular flux is considered in a limited number of directions, and it is assumed to vary in a linear manner between these discrete directions. The symbol S_N is commonly used to describe the discrete ordinates method, where S stands for segments and N is the number of directions. The accuracy attainable increases with N because a better approximation of the actual angular flux distribution is possible, but so does the complexity of the computations. In practice, S_4 approximation has been found to be satisfactory for most purposes, although S_8 and S_{16} have sometimes been used [3,19]. The S_N expression in terms of discrete directions applies only to the angular neutron flux distribution in space.

For this work, the quadrature weight of S_8 was selected in order to attain greater accuracy. The P_3 scattering order was selected for the cylindrical geometry pertaining to GHARR-1 reactor.

By discretising the angular variable into a number of discrete directions, the angular fluxes are calculated using a set of μ values and carrying out all integrations by a quadrature scheme, so that

$$\int_{-1}^{1} f(\mu)d\mu = \sum_{m=1}^{M} \mu_m f(\mu_m) \tag{11}$$

Discrete ordinate quadrature set Ω_m and w_m weights are selected to discretise the transport equation. The approximate value of the integral is

$$\int_{\hat{\Omega}} \Phi(\vec{r},\hat{\Omega})d\hat{\Omega} = \sum_{m=1}^{M} \Phi(\vec{r},\hat{\Omega})w_m \tag{12}$$

The quadrature weights w_m and μ_m form part of the data for the problem. The solution has to satisfy the principles of (i) physical symmetry and (ii)the arrangement of discrete directions on latitudes on the unit sphere, [20] have details on discrete ordinate angular quadratures.

For 1-D geometries, the following underlisted criteria must be satisfied by the quadrature sets w_m and μ_m;

(a) invariance projection, that is, μ_m must be symmetric about $\mu = 0$, or $\mu_i = -\mu_{m+1-i}$, and $w_i = w_{m+1-i}$ (Symmetric upon reflection).

(b) positivity of the solution, that is, $w_m > 0$ with the condition

$$\sum_{m=1}^{M} w_m = 1 \tag{13}$$

Using conditions (a) and (b) means that

$$\sum_{m=1}^{M} \mu_m w_m = 0.$$

ANISN code employs the quadrature scheme which satisfies conditions (a) and (b). In addition, the diffusion theory condition must be satisfied;

$$\sum_{m=1}^{M} w_m \mu_m{}^2 = \frac{1}{3} \tag{14}$$

The full discretized multigroup discrete ordinate 1-D equation with isotropic scattering ($l = 0$) for geometries of slab, cylinder and sphere can be written in the general form as

$$\mu_m (A_{i+\frac{1}{2}} \Phi^g_{m,i+\frac{1}{2}} - A_{i-\frac{1}{2}} \Phi^g_{m,i-\frac{1}{2}}) + (a_{m+\frac{1}{2}} \Phi^g_{m+\frac{1}{2},i} - a_{m-\frac{1}{2}} \Phi^g_{m-\frac{1}{2},i}) / w_m$$

$$\sum_{t,i}^{g} \Phi^g_{m,i} V_i = S^g_{m,i} V_i \tag{15}$$

i=1,2,3,...,I, m=1,2,...,M,
where the area A and volume V for slab, cylindrical and spherical geometries are given in Table 3.1 below

Table 3.1 [6]

Geometry	$A_{i\pm\frac{1}{2}}$	V_i
1-D slab	1	∇X_i
1-D cylinder	$4\pi r^2_{i\pm\frac{1}{2}}$	$4\pi r_i^2 \nabla r_i$
1-D sphere	$2\pi r_{i\pm\frac{1}{2}}$	$2\pi r_i \nabla r_i$

The curvature coefficient, a, is obtained from the recurrence relation

$$a_{m+\frac{1}{2}} = a_{m-\frac{1}{2}} - \mu_m w_m (A_{i+1} - A_i) \qquad (16)$$

with

$$a_{\frac{1}{2}} = a_{m+\frac{1}{2}} = 0.$$

the centre fluxes are related to the edge fluxes such that

$$\Phi^{g}_{m,i} = \alpha \Phi^{g}_{m,i+\frac{1}{2}} + (1-\alpha)\Phi^{g}_{m,i-\frac{1}{2}}$$

$$\Phi^{g}_{m,i} = \alpha \Phi^{g}_{m+\frac{1}{2},i} + (1-\alpha)\Phi^{g}_{m-\frac{1}{2},i}, \qquad \text{i=1,2,...,I and m=1,2,3,...,M.}$$

The diamond scheme ($\alpha = \frac{1}{2}$) is used in ANISN.

3.1.2. Matrix Equation.

After discretizing the transport Eqn.(9) into discrete phase-space cell, a resulting system of an algebraic equation at discrete mesh points for energy group g, is obtained. The matrix form is presented as

$$\mathbf{A\Phi = B\Phi + S} \qquad (17)$$

where

$\mathbf{A}$ is a matrix representing the streaming-collision operator $\Omega.\nabla + \sum$

$\mathbf{B}$ is a matrix representing the group in-scattering term.

$\mathbf{S}$ is a matrix representing the external, plus group-to-group scattering sources, including fission.

Φ is the angular flux vector.

The direct solution of the matrix equation by inversion of $(\mathbf{A} - \mathbf{B})$ is not feasible and uneconomical. Instead a dual strategy is employed which consists of two nested iterations; outer and inner iterations, fig 3.1. The outer iteration scheme sweeps through all energy groups in the order of decreasing energy and thus provides an updated value of the flux for the entire system [15]. This is accompanied by splitting the matrix B into four parts as

$$\mathbf{B} = \mathbf{B}^{s} + \mathbf{B}^{u} + \mathbf{B}^{d} + \mathbf{B}^{f} \tag{18}$$

where $\mathbf{B}^{s}$ is the in-group scattering, $\mathbf{B}^{u}$ for upscattering, $\mathbf{B}^{d}$ for downscattering and $\mathbf{B}^{f}$ is for fission. Thus, the outer iterative scheme becomes

$$(\mathbf{A} - \mathbf{B}^{d} - \mathbf{B}^{s})\Phi^{n} = (\mathbf{B}^{u} + \mathbf{B}^{f})\Phi^{n-1} + \mathbf{S} \tag{19}$$

The old flux Φ^{n-1} is used to calculate the upscattering and fission contributions using Eqn. (19) and the new flux Φ^{n} is calculated by solving the last equation group-by-group.

The presence of self scattering term $\mathbf{B}^{s}$ makes direct inversion of the matrix $(\mathbf{A} - \mathbf{B}^{d} - \mathbf{B}^{s})$ impractical therefore the following inner procedure is applied;

$$\mathbf{A}_{gg}.\Phi_{g}^{n,k} = \mathbf{B}_{gg}^{s}.\Phi_{g}^{n,k-1} + \mathbf{Q}_{g}^{n} \tag{20}$$

where

$\Phi_{g}^{n,k}$ is a vector whose components are values of the angular flux in group g for the space and angular mesh for outer iteration n and inner iteration k. The source $\mathbf{Q}_{g}^{n}$ is the within group source

$$\mathbf{Q}_g^n = [\mathbf{B}^d \Phi^n + (\mathbf{B}^u + \mathbf{B}^f)\Phi^{n-1} + \mathbf{S}]_g \tag{21}$$

The source is calculated with the most recently available fluxes which means that the downscattering term uses fluxes from the outer iteration while the upscattering and the fission contributions are computed from the flux in the previous outer iteration. This implies that the effective source and the previous estimate for the within group flux $\Phi_g^{n,k-1}$ are used to sweep through all the directions and regions to calculate $\Phi_g^{n,k}$.

For multiplying medium, the effective factor, K_{eff} is included in Eqn.(19) and in the absence of external source, the equation becomes

$$\mathbf{A}\Phi = [\mathbf{B}^u + \mathbf{B}^s + \mathbf{B}^d]\Phi + \lambda^{-1}\mathbf{B}^f\Phi \tag{22}$$

The procedure as presented above is applicable for its solution.

There are two options for convergence test that are available;

(i) integral convergence which is expressed in the form

$$\frac{1}{v}\int\{\frac{\Phi^n - \Phi^{n-1}}{\Phi^n}\}dv < \varepsilon \tag{23}$$

and

(ii) the pointwise convergence criteria;

$$\max[\frac{\Phi^n - \Phi^{n-1}}{\Phi^n}] < \varepsilon \tag{24}$$

The simplified flow chart of multigroup calculation for ANISN code [6] is shown in fig.3.1.

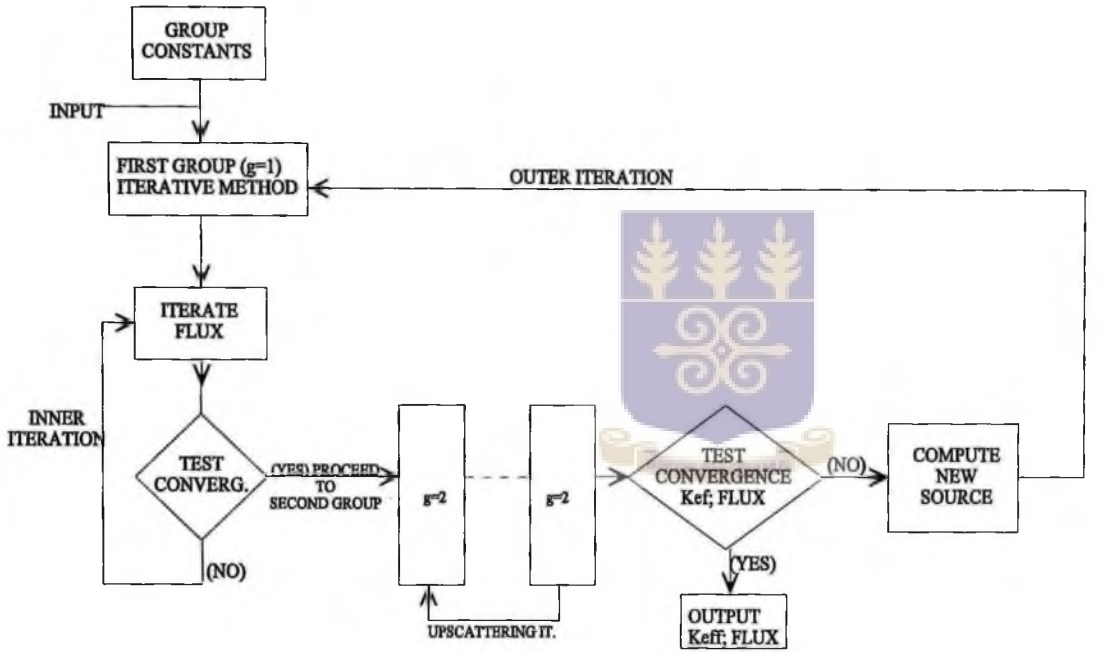

FIGURE 3.1BLOCK DIAGRAM OF A MULTIGROUP CALCULATION

3.2. NEUTRON AND GAMMA SOURCE DISTRIBUTION

The microscopic cross-sections of materials of various regions through which neutron and gamma rays pass were extracted from a master library named VITAMIN C, consisting of 171 neutron energy and 36 gamma-ray energies. The sources which enter the code from the basic data of ENDF/B file through the 17^{**} card were obtained using the utility code GENSOU, Fig.3.2 also incorporated into MTR_PC package. The primary sources of neutrons and gamma rays produced in the core could be classified into three categories;

(i) Fission Neutrons;

$$S_N^g = \frac{p(r)}{E_f} \nu \chi_g \qquad (25)$$

where

$p(r)$ = total number of neutrons emitted by thermal fission.

ν = mean number of neutrons produced.

χ_g = fraction of neutrons emitted by fission.

E_f = amount of energy released per fission.

(ii) Prompt fission Gamma Rays;

$$S_\gamma^g = \frac{p(r)}{E_f} \Gamma_F^g \qquad (26)$$

where

Γ_F^g is the number of gammas emitted in the energy group per fission and calculated using spectrum [21].

$$\Gamma(E) = \begin{cases} 6.6; 0.1 < E < 0.6 Mev \\ 20.2\exp(-1.78E); 0.6 < E < 1.5 Mev \\ 7.2\exp(-1.09E); 1.5 < E < 10.5 Mev \end{cases}$$

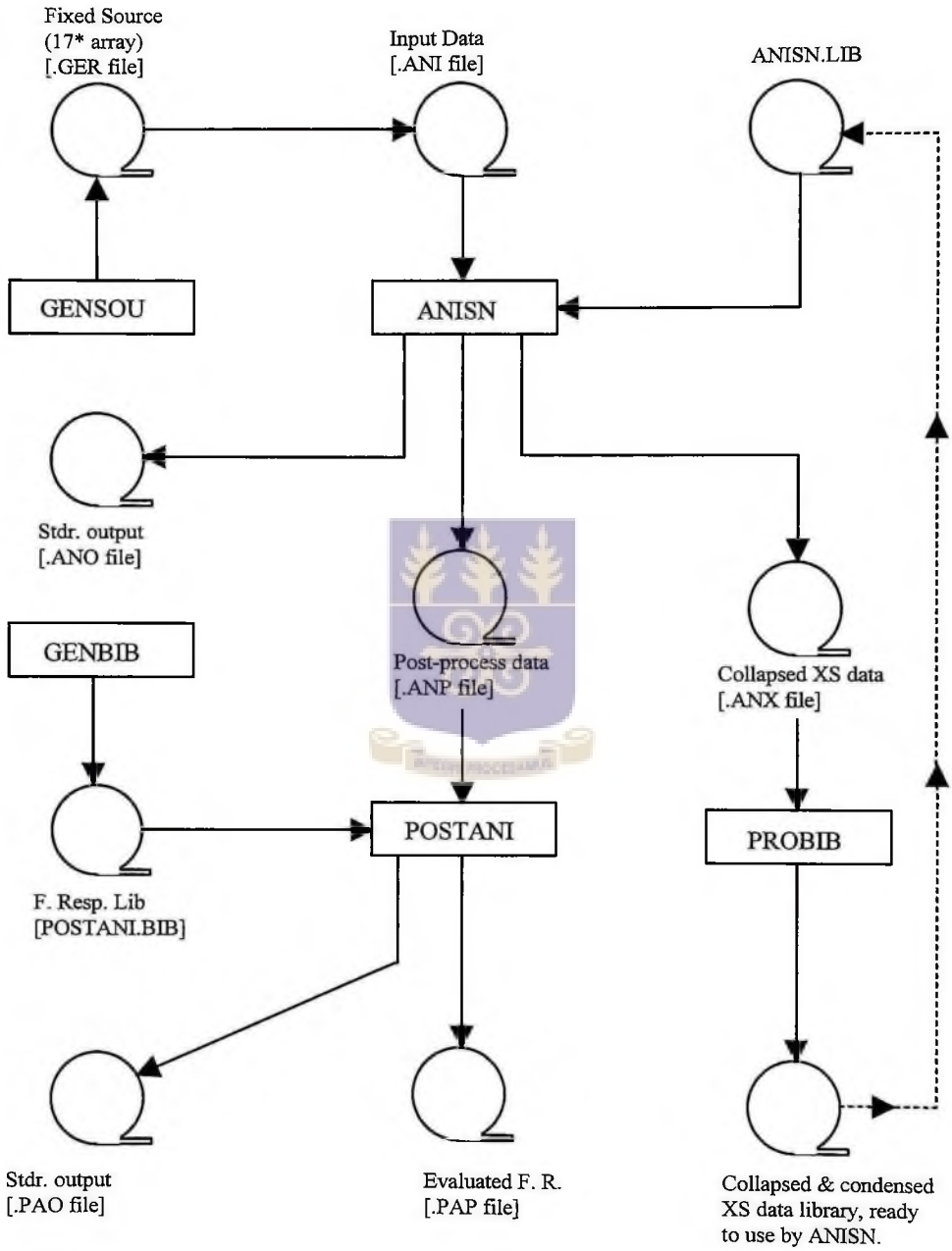

Fig. 3.2 ANISN utility programs: Flowchart.

(iii) Scattering of Neutrons and Photons;

$$S_s^g(r) = \sum_{g \to g'} \Phi_g \qquad (27)$$

where g = 1,2,3,...,171(g' = 172,173,...,207)

and $\sum_{g \to g'}$ is the macroscopic scattering cross-section and Φ_g is the flux which is dependent on the reactor power.

The concentrations of elements in various regions were computed on procedures outlined in the manual of WIMSD/4 [22]and reported by [23] for neutronic calculations of the reactor.

CHAPTER 4

NEUTRONS AND GAMMA DOSE RATES FOR NORMAL OPERATIONAL CONDITIONS

This Chapter deals with the theoretical calculation of dose rates at various regions and positions in the reactor GHARR-1 using the 1-D ANISN transport computer code. Experimental measurements were also carried out to validate the calculated results. Based on the validated results, further theoretical calculations such as the determination of the variation of dose rates around and along the slant tubes in the reactor and the estimation of neutron and gamma dose rates for loss-of-coolant accidents were also carried out and presented in this Chapter and Chapter 5 respectively.

A brief description of GHARR-1 for which the present work is being conducted is presented in Section 4.1 followed by reactor shield analysis for normal operational states.

4.1. DESCRIPTION OF GHARR-1 REACTOR

GHARR-1 is a 30kW low power research reactor. It is designed and manufactured by the China Institute of Atomic Energy. The reactor is similar in design to the Canadian SLOWPOKE-2. It is a tank-in-pool reactor which is operated and utilized for Neutron Activation Analysis (NAA) in a large number of fields like mineral exploration, medicine, agriculture, environment, food and industry. It also finds use in other areas such as in short-lived radioisotope production, research, teaching and training. Its maximum licensed power is 30kW with thermal neutron flux inside the inner irradiation site of $1 \times 10^{12}\ \mathrm{n/cm^2.s}$. The vertical cross section of the reactor is shown in Fig.4.1 and the layout of the reactor complex can be seen in Fig.4.2.

The main specifications of the reactor are tabulated in Table 4.1. The fuel cage of the reactor which is located on a Be plate is also surrounded by a Be reflector to ensure effective shielding. On top of the core is placed an Al tray which may contain some quantities of Be plates with known thickness depending on the duration of operation. The core of the reactor is located at the lower section of the reactor vessel of height 0.9m. The upper vessel of the reactor container is 4.7m. The reactor vessel is suspended on a square bracket in a stainless steel lined pool of diameter 2.7m. The reactor container and pool which is embedded in reinforced concrete of 40cm thickness are filled with deionized water to specified levels as shown in Fig.4.3 to provide shielding from radiation during reactor operation.

There is a gas space of 44.5cm above the water in the vessel for radioactive gases such as H_2, O_2, and Ar which are purged weekly. All these designs are to ensure effective shielding of radiation hence the inherently safe nature of the reactor [21].

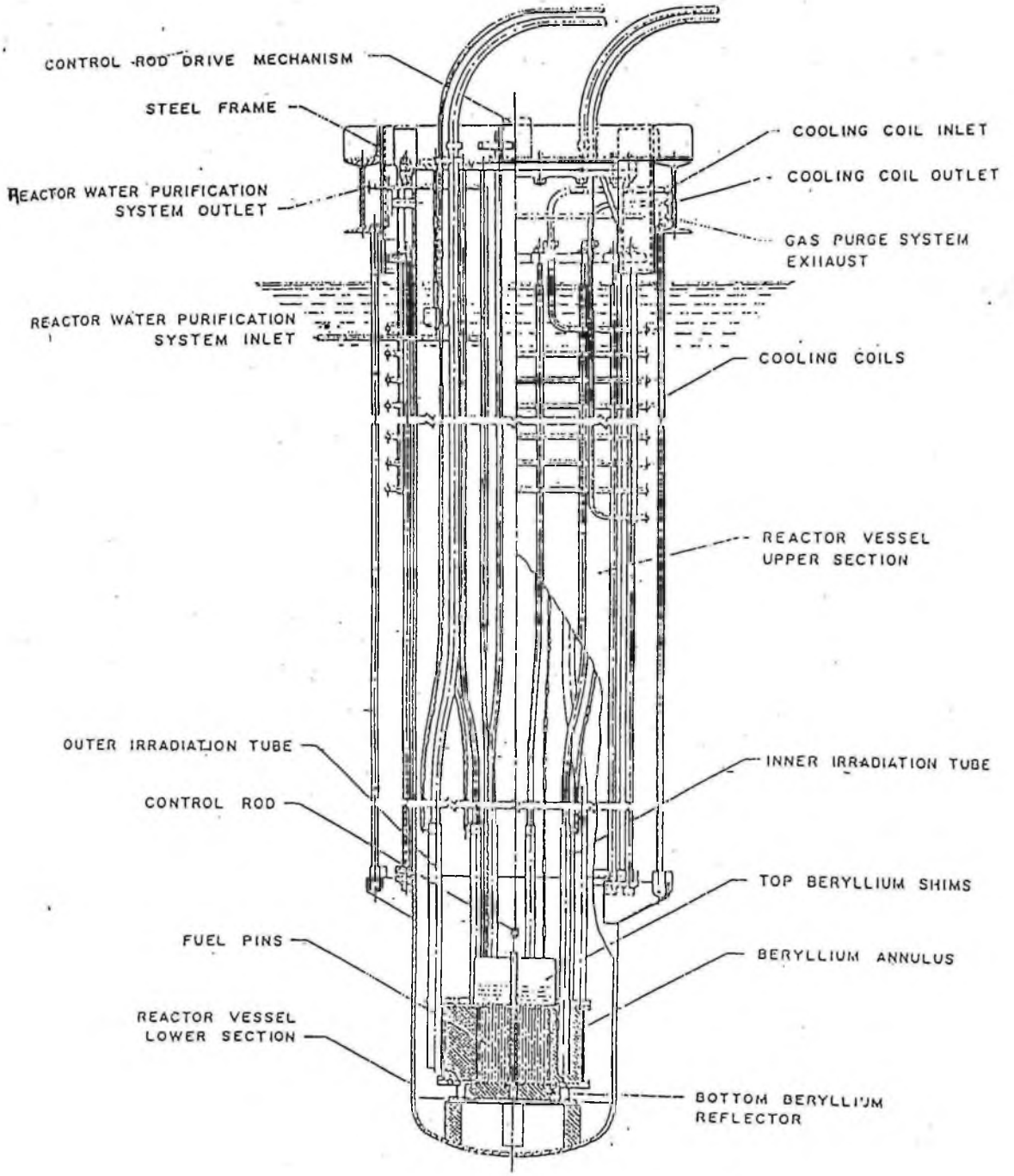

Fig. 4.1 Vertical cross section of GHARR-1 vessel and its components

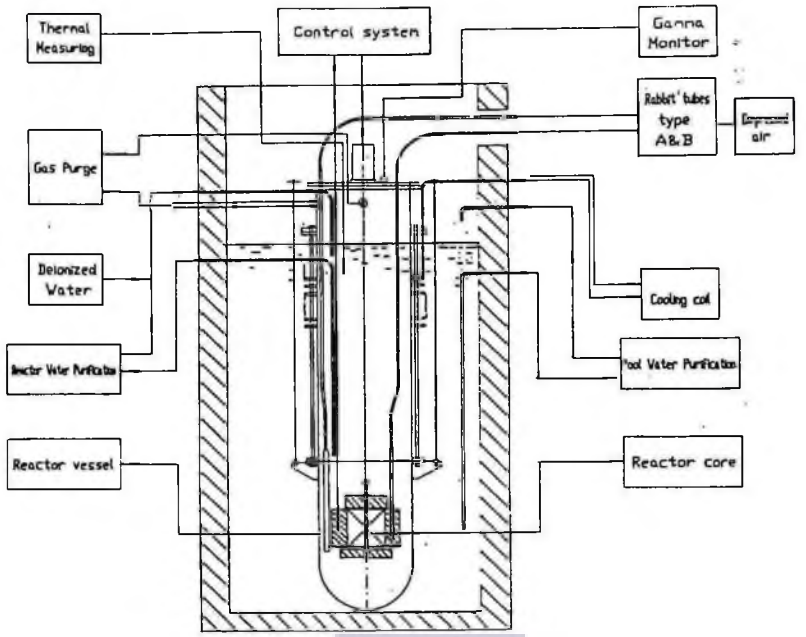

Fig.4.2. GHARR-1 Reactor and its Systems.

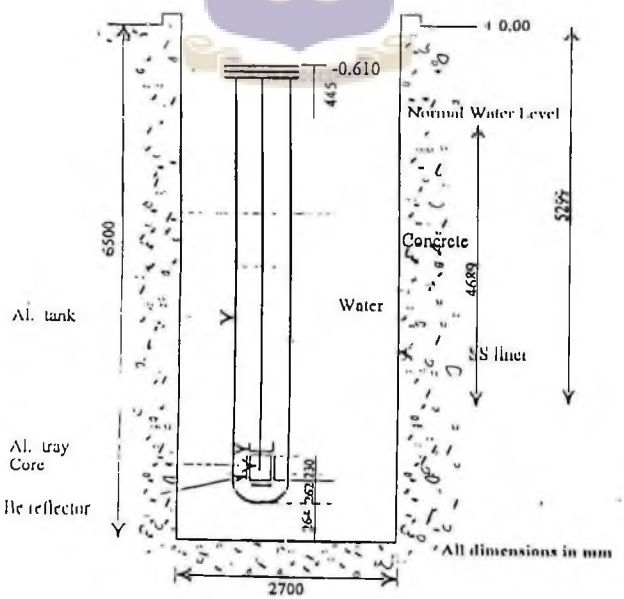

Fig. 4.3. Reactor Vessel and Pool with Deionized Water.

Table 4.1; Main Specifications of GHARR-1 [21,24]

Parameters	Description
Reactor Type	Tank-in-pool
Rated thermal power	30kW
Fuel	UAl_4 dispersed in Al base material
U-235 enrichment	90.2%
Core shape	Cylinder
Core diameter	23cm
Core height	23cm
Fuel element shape	Thin rod
Fuel element number in the core	344
Total weight of U	1106.559g
Total weight of U-235	998.116g
Reactor continuous operating time(at rated power)	6.5hours
Refuel period	More than ten years
Burnup	~1%
Temperature coefficient	~-0.10mk/degree Celsius (average)
Control rod (Cd)	One in the centre of the core
Total number of irradiating sites	10
Number of inner irradiating sites	5
Thermal neutron flux (at rated power in inner irradiation sites)	$1.0 \times 10^{12} n / cm^2 . s$
Number of outer irradiation sites	5 (2 larger, 3 smaller)
Thermal neutron flux (at rated power in outer irradiation sites)	$\sim 5.0 \times 10^{11} n / cm^2 . s$

Height of outlet orifice	7.5mm
Inner diameter of annular Be	23.1cm
Outer diameter of annular Be	43.5cm
Height of annular Be	23.85cm
Thickness of bottom Be plate	5.00cm

4.2. THEORETICAL CALCULATIONS

The 1-D code ANISN, was applied to estimate the neutron and gamma dose rates at various regions and positions in the reactor as shown in Fig.4.4. The various material regions of the reactor showing the dimensions through which particles are transmitted are shown in Table 4.2.

The instructions for preparation of input data listed in Appendix A were followed in accordance with procedures and method of analysis for the code ANISN discussed in Chapter 3

In order to use the 1-D transport code for the determination of the variation of dose-rate around and along the slant tubes and for the estimation of dose rates during loss-of-coolant accidents, it was decided to validate the code with experimental data. The experimental procedures and measured results in comparison to computed results are presented below.

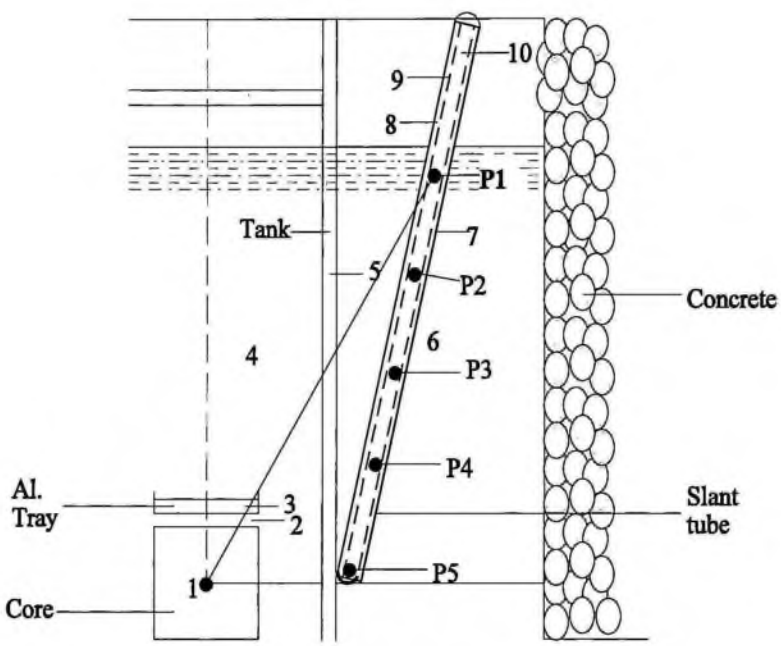

Fig.4.4 Regions and Positions in the reactor and the slant tube

Table 4.2 The regions of the reactor and the slant tube

REGIONS	MATERIALS	THICKNESS /cm
1	Fuel	12.51
2	Aluminium + Water	0.33
3	Aluminium Tray	1.20
4	Water	52.68
5	Aluminium Tank	2.54
6	Water	8.40
7	Slant tube	0.19
8	Air	1.00
9	Aluminium Tube	0.19
10	Air	1.81

4.3. VALIDATION OF THE CALCULATED VALUES WITH EXPERIMENTAL DATA

Radiation monitoring equipment which were used during on-site critical and full power experiments at the GHARR-1 Centre, were to measure the gamma and neutron dose rates respectively. The SG102 monitor is fitted with an external NaI detector for the detection of the gamma-radiation and is recorded on its analog meter. The instrument has an outlet in which the analog signal was converted to a digital signal through a multimeter for precise recording to be made to higher significant figures. The range of measurement is 0-10 μ Sv/hr.

The NH-1A neutron monitor is made of a 22.5cm diameter cadmium-loaded polyethylene sphere with a BF_3 counter in the center of the sphere and is used to measure the neutron dose equivalent from the neutron detection reaction $^{10}B(n,\alpha)^{7}Li$. The full scale deflection of the analog meter is 10^4 μ Sv/hr and that of the digital counter is 999counts.

Measurements at the top of the reactor at various positions are shown by the alphabets in Fig.4.5. Because of the limited range of the SG102 monitor, experimental determination of gamma dose rates were carried out at the following positions:

(i) along the midplane of the core to the concrete shield beyond the liner of the pool.

(ii) at the edge of the pool liner.

(iii) at the edge of the reactor vessel.

(iv) at the centre line of the reactor vessel.

Gamma dose rates were also checked against those recorded by Radiation Alert Monitor-4 with range 0-5mSv/hr and four halogen counter type J613 γ GM probes with readout on the gamma radiation monitoring system of the control console and the microcomputer control system. No significant level of neutron dose rate was measured due to the effective shielding provided by water in the reactor vessel and pool.

The calculated results of the ANISN code has been validated using experimental results in order to set standard procedures to be applied in future studies. In developing such a standard method, the errors to the final results of the dose rates from the centre of the core to the edge of the reactor pool have been quantified. The computed and experimental results of the average gamma dose rates recorded at 30kW and at different reactor power levels are listed in Tables 4.3 and 4.4 respectively.

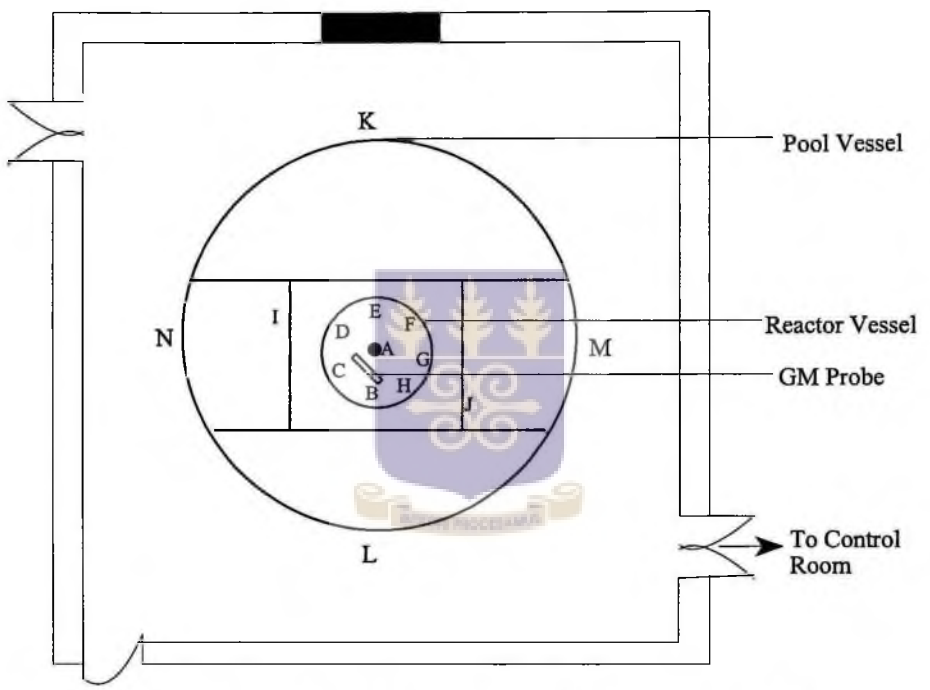

Fig. 4.5 Positions at the top of the Reactor in the Reactor Hall.

Table 4.3 Comparison of Calculated and Experimental Gamma Dose Rates

Distance from centre of Reactor Core /cm	Calculated Value/ $\mu Sv / hr$	Experimental Value/ $\mu Sv / hr$	%Variation	Standard Deviation
162	25.83	25.00	3.32	0.59
102	25.83	24.00	7.63	1.29
44	79.10	80.00	1.13	0.64
0	79.30	80.00	0.88	0.49

Table 4.4. Comparison of Calculated and Measured Gamma Dose Rates for Different Reactor Power Levels

Neutron Flux / $n / cm^2 .s$	Reactor Power/ kW	Calculated Dose Rate/ $\mu Sv / hr$	Measured Dose Rate/ $\mu Sv / hr$	% Variation	Standard Deviation
1.0×10^9	0.03	7.84E-02			
1.0×10^{10}	0.3	7.90E-01	7.80E-01	1.28	0.01
1.0×10^{11}	3.0	7.90E+00	7.30E+00	8.21	0.42
2.5×10^{11}	7.5	1.88E+01	1.875E+01	0.27	0.04
5.0×10^{11}	15.0	3.96E+01	4.00E+01	1.00	0.28
8.0×10^{11}	24.0	6.33E+01	6.50E+01	2.62	1.20
1.0×10^{12}	30.0	7.90E+01	8.00E+01	1.25	0.71

It can be seen from Tables 4.3 and 4.4 that the calculated results approximately agreed with the experimental data with a maximum percentage variation of 8.21 and standard deviation of 1.29.

Fig.4.6 shows the calculated dose rates operating for 30kW power for neutron and gamma (n+g), neutron only (n) and gamma only (g) as a function of radial distance from the centre of the core to the concrete. A drastic reduction of dose rates from the annular Be reflector through the water, the stainless steel liner and the concrete was noticed. The dose rate at the end of the 40cm thick concrete

is very low suggesting that shielding is very effective in that direction. The earth surrounding the pool provides additional attenuation effect for the neutrons and the gamma rays. The variation of the dose rates with distance from the core to the edge of the pool, shown in Fig.4.7 at an operating power of 30kW indicates similar trend. The computed results reproduced the tendency in the experimental results as shown in Fig.4.8.

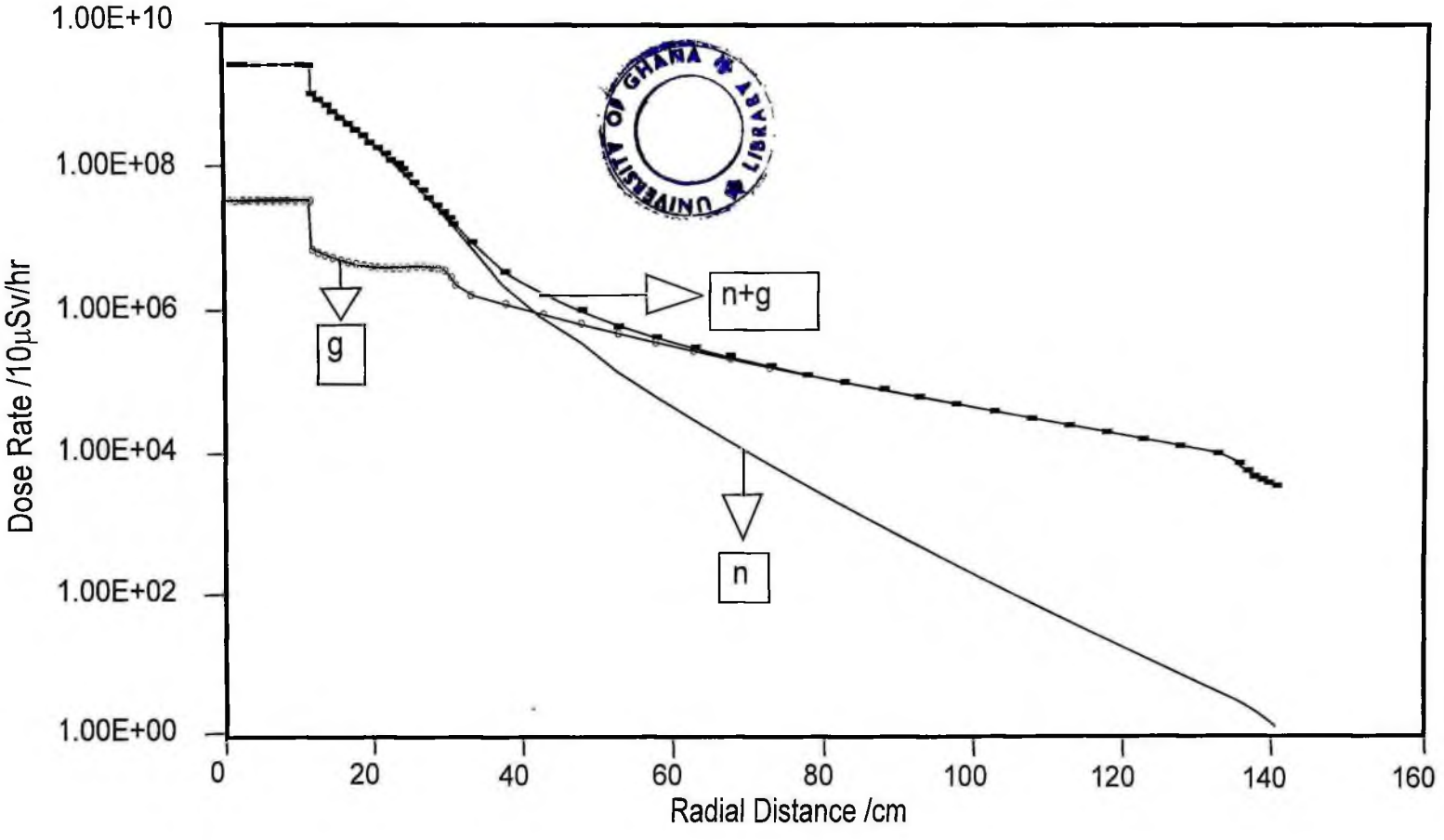

Fig.4,6 Variation of Dose Rates with Radial Distance from midplane of core to the concrete.

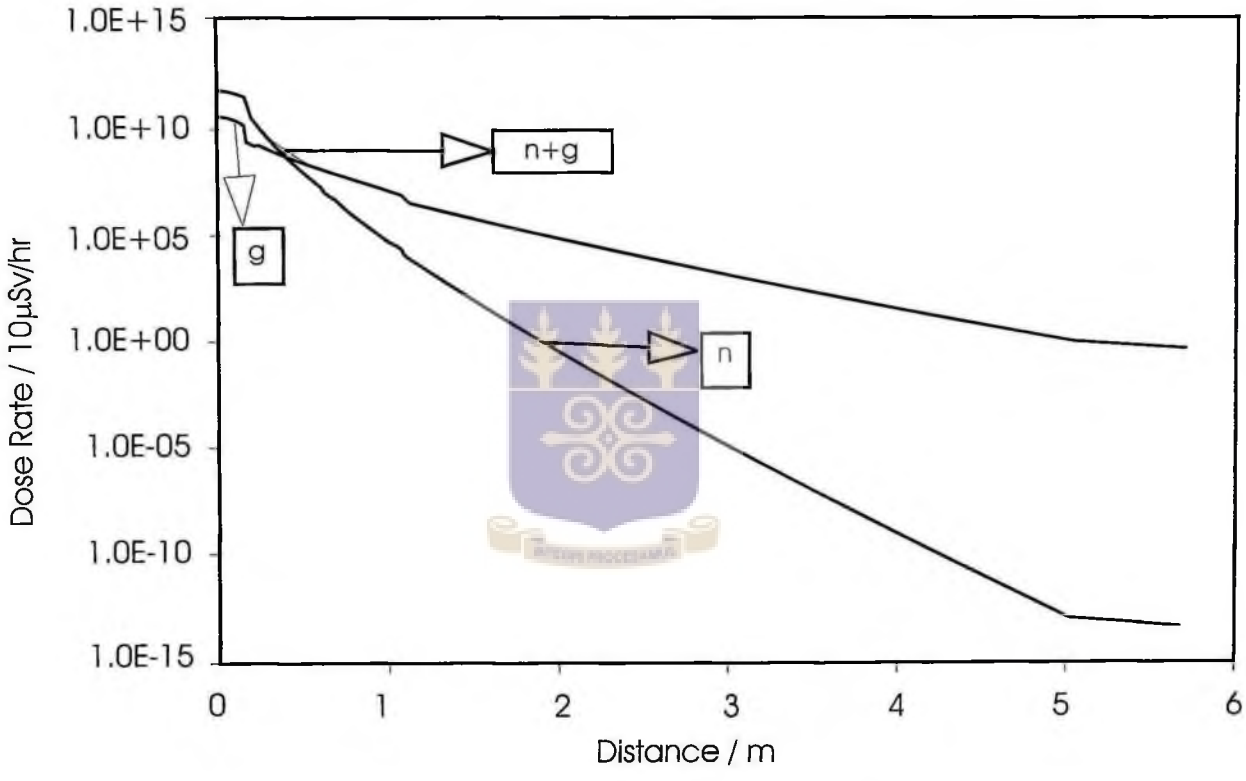

Fig.4.7 Variation ofDose Rates from Centre of Core to the pool

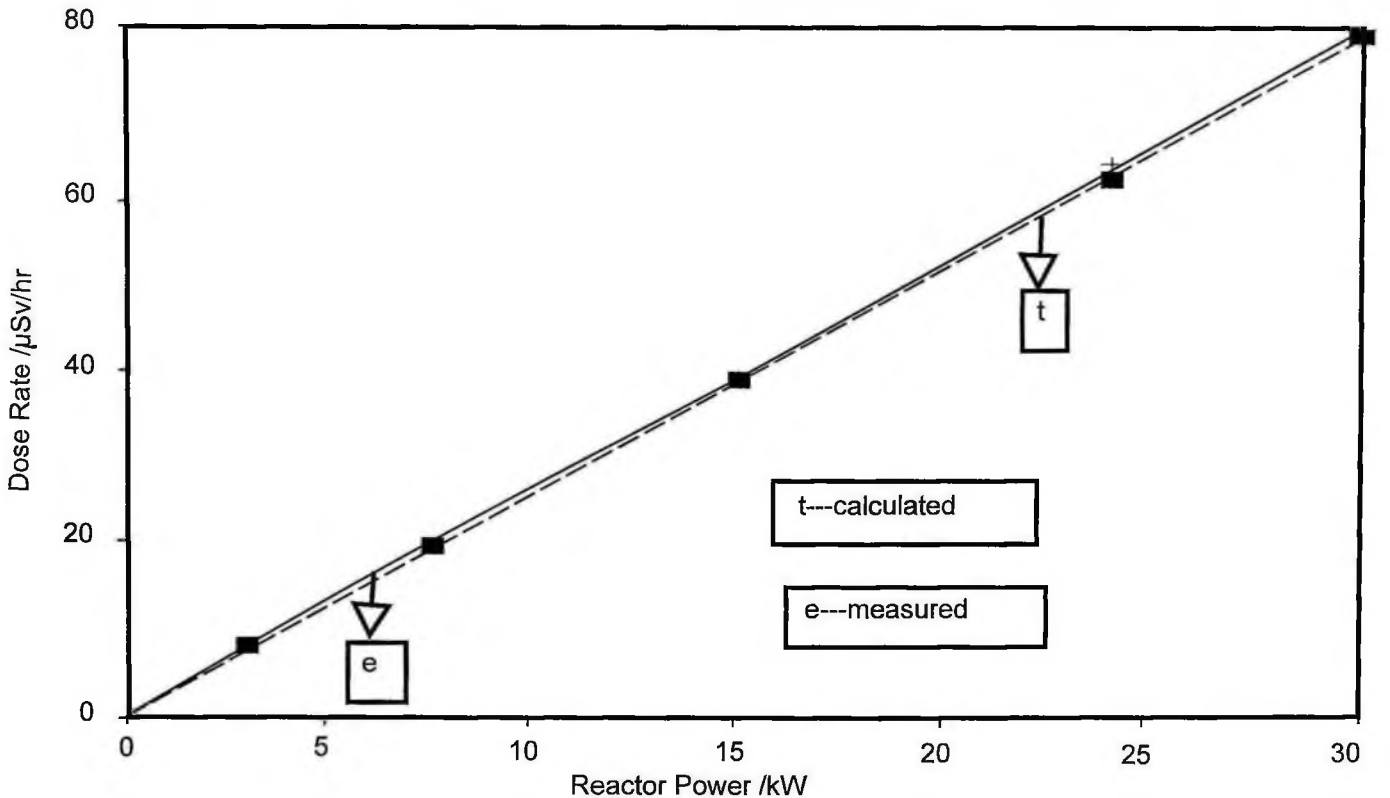

Fig 4.8 Gamma Dose Rates for Different Reactor Power Levels

4.4. DOSE MAPPING ALONG THE SLANT TUBES.

Two slant tubes are attached to the lower section of the reactor vessel in the region of the core. The tubes were used to commission the reactor in December, 1994. After the commissioning, the slant tubes became part of the reactor. It is envisaged that the tubes can be used to study the effect of neutron or gamma irradiation on mutation breeding of seeds. There is the need therefore to study the variation of dose rates along and within the tubes for future mapping.

Following the procedure in the manual for ANISN input preparation [9], five main positions P1 to P5, in the slant tubes, as shown in Fig.4.4, were selected and the dose rates calculated to study the variation of dose rates from the core to these positions. The main material regions of the reactor and the slant tube showing the dimensions for a typical input data are contained in Table 4.2 shown above. The dose profile within the slant tube from the bottom P5 to the top P1, was also calculated. All the calculations were carried out for maximum thermal power of 30kW.

The results of the variation of dose rate with distance from the core to the P positions, and within the slant tubes are also presented. The distribution of neutron + gamma (N+G), neutron only(N) and gamma only(G) shown in Figs.4.90 to 4.92, follow similar trend as the validated results. The neutron population in the core of the reactor is far higher than that of the gamma but decreases drastically from P4 to P1. The reason might be that the neutrons are much more attenuated by the water and the various media on the paths. However, at position P5 in the slant tube, the presence of neutrons is much more prevalent than the gammas. This might be due to the very small amount of water and other few attenuating agents such as beryllium and the reactor vessel on the path from the core. Another contributing factor might be the very short distance from the core to the P5 position. Along the slant tube, there is an increase in the gamma dose rate from about 1.50Sv/hr at position P5 to about 2.50Sv/hr at P4, and a slow decrease thereafter to almost 0Sv/hr at position P1 as shown in Fig. 4.93. The trend between P5 and P4 might be due to the dominance of the neutron. The dominance of the gamma from position P4 to P1 might largely be due to its penetrating power compared to that of the neutron which is low, especially with the increase in the water thickness from the reactor core as shown in Fig. 4.94. The fast neutrons that escape from the reactor core are slowed down due to scattering collision. If the collisions are of the inelastic type, the process will be accompanied by inelastic scattering gamma rays [8,17,25,26]. These scattering gamma rays might constitute the major part of the secondary radiations in these positions. The distribution of the neutron + gamma (N+G), at the P positions is also shown in Fig.4.95.

With this available information on the variation of the neutron and the gamma doses along the slant tube, high dose thermolumniscent (TLD) badges could be used to confirm the calculated values. Consequently, the tubes could be mapped properly to pave way for the study on the effect of gamma or neutron irradiation on mutation breeding of seeds in the field of agriculture.

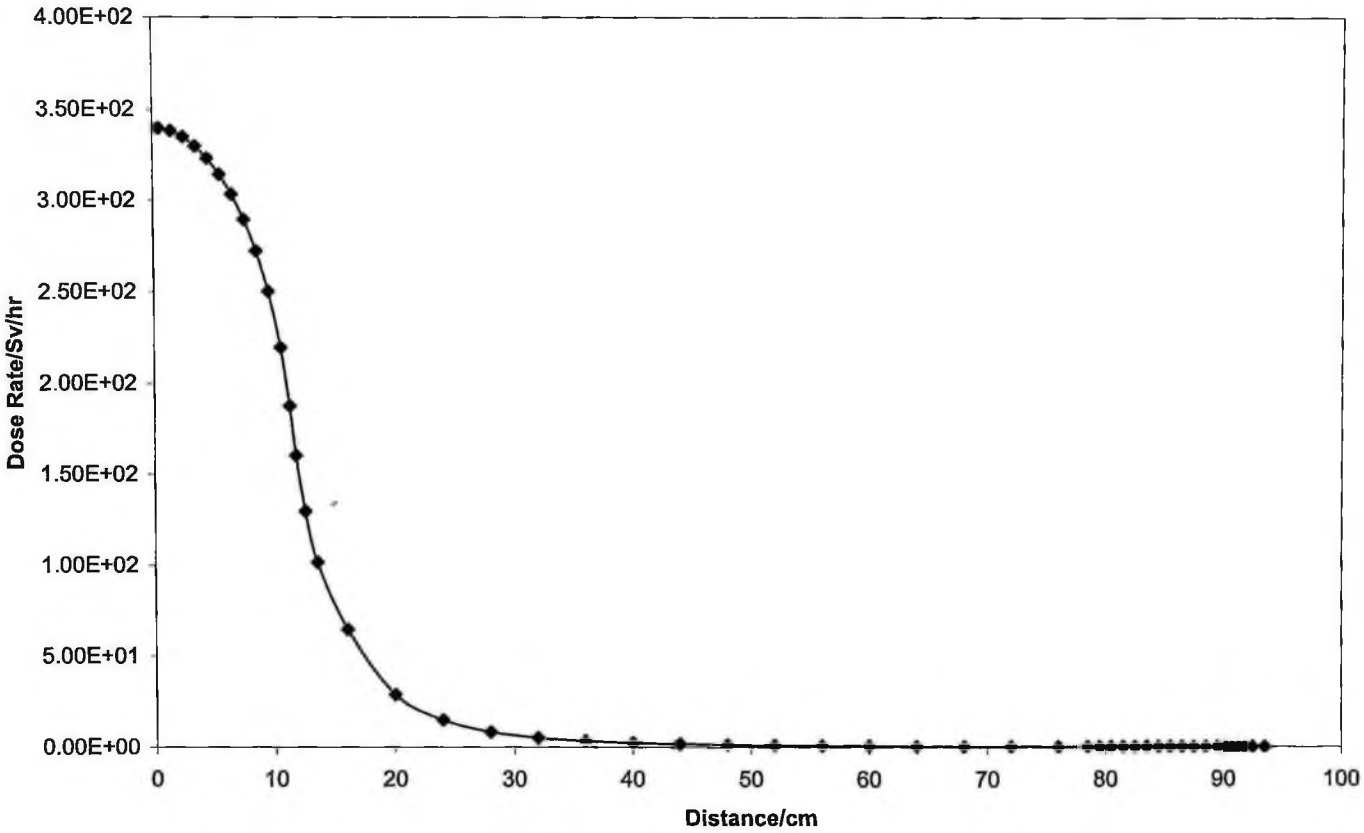

Fig. 4.90 Variation of N+G Dose Rate with Distance from Midplane of the Core to position P1 in the slant tube.

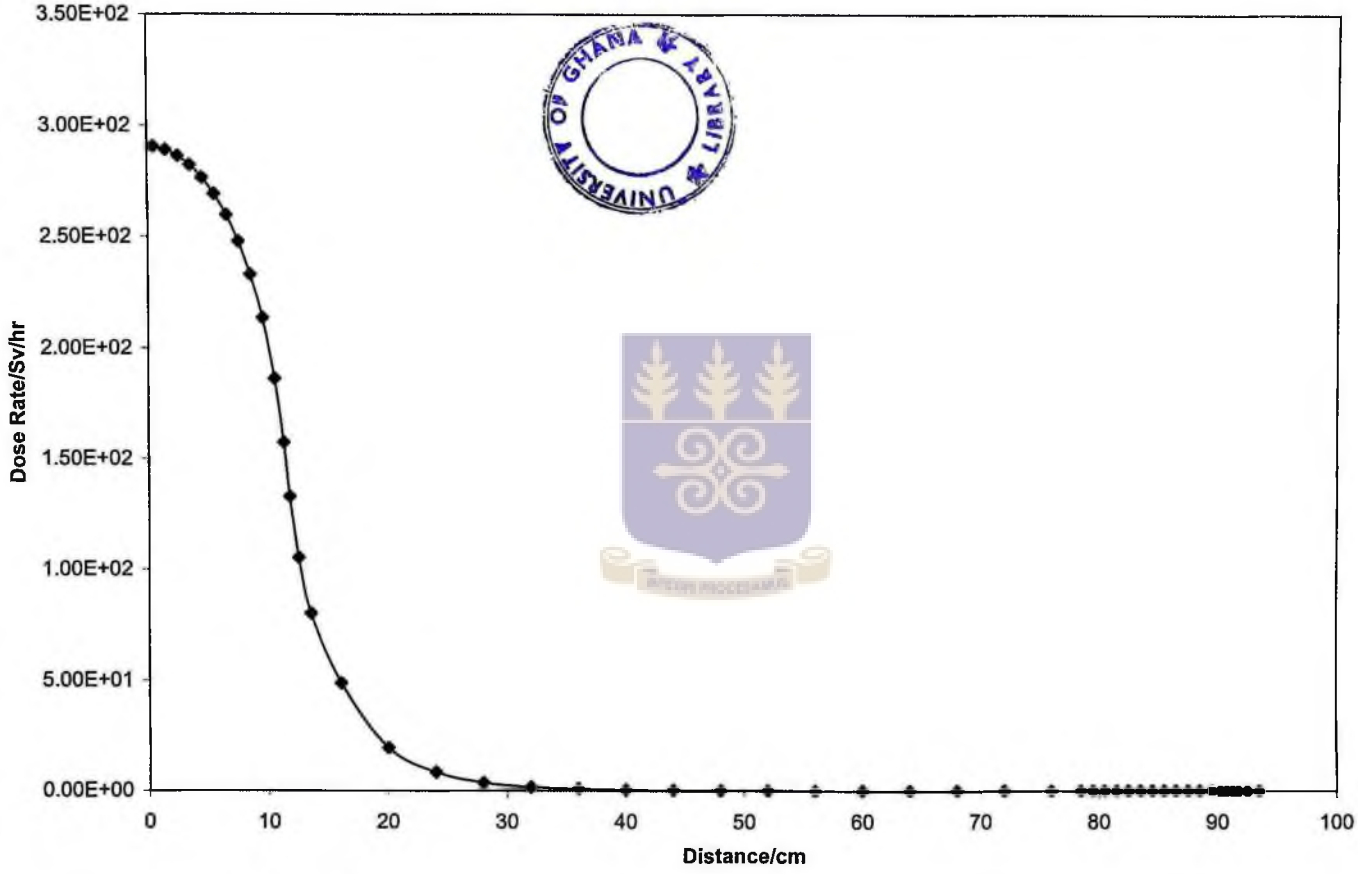

Fig. 4.91 Variation of Neutron Dose Rate with Distance from Midplane of Core to position P1 in the slant tube.

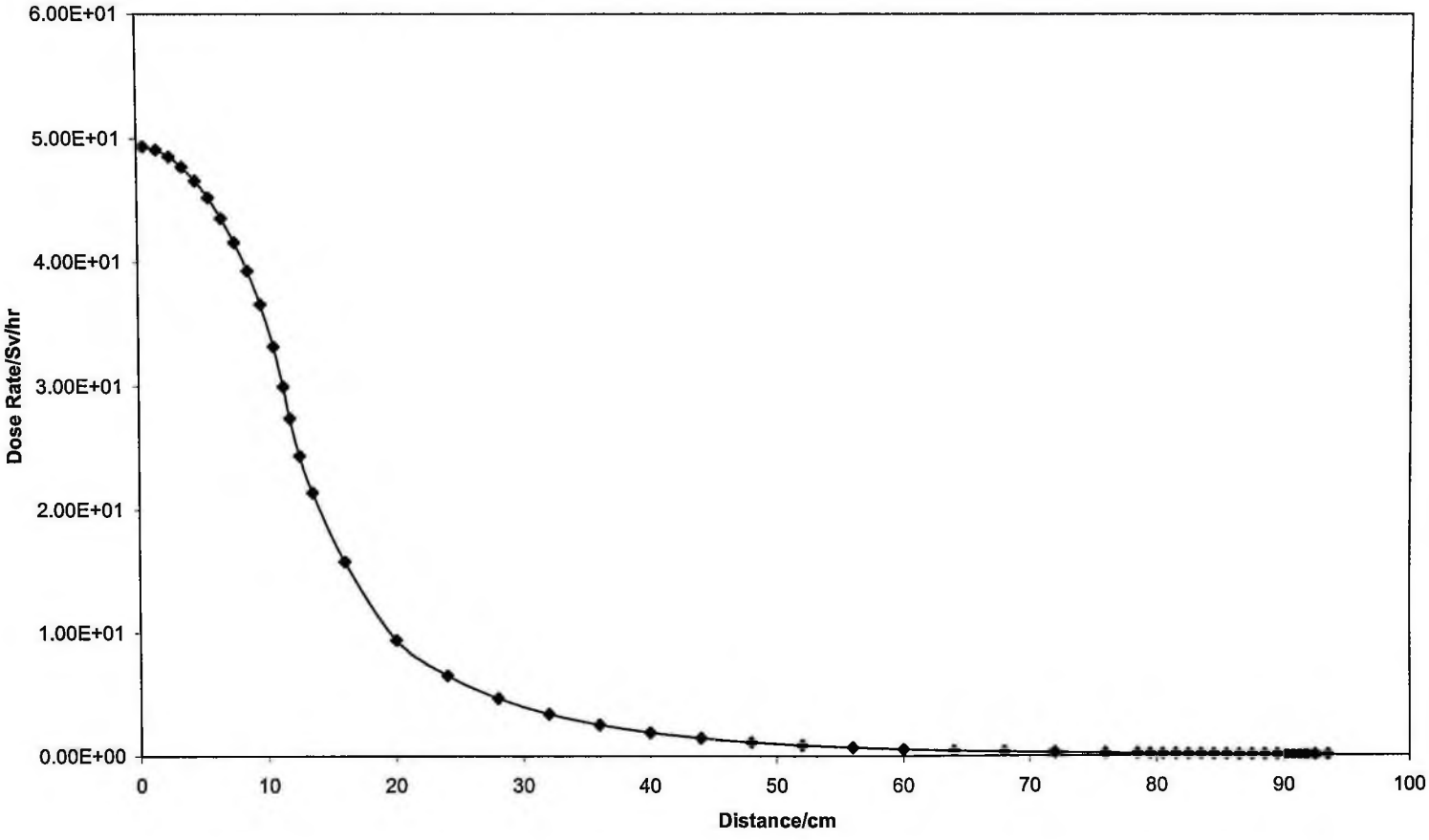

Fig. 4.92 Variation of Gamma Dose Rate with Distance from Midplane of Core to position P1 in the slant tube.

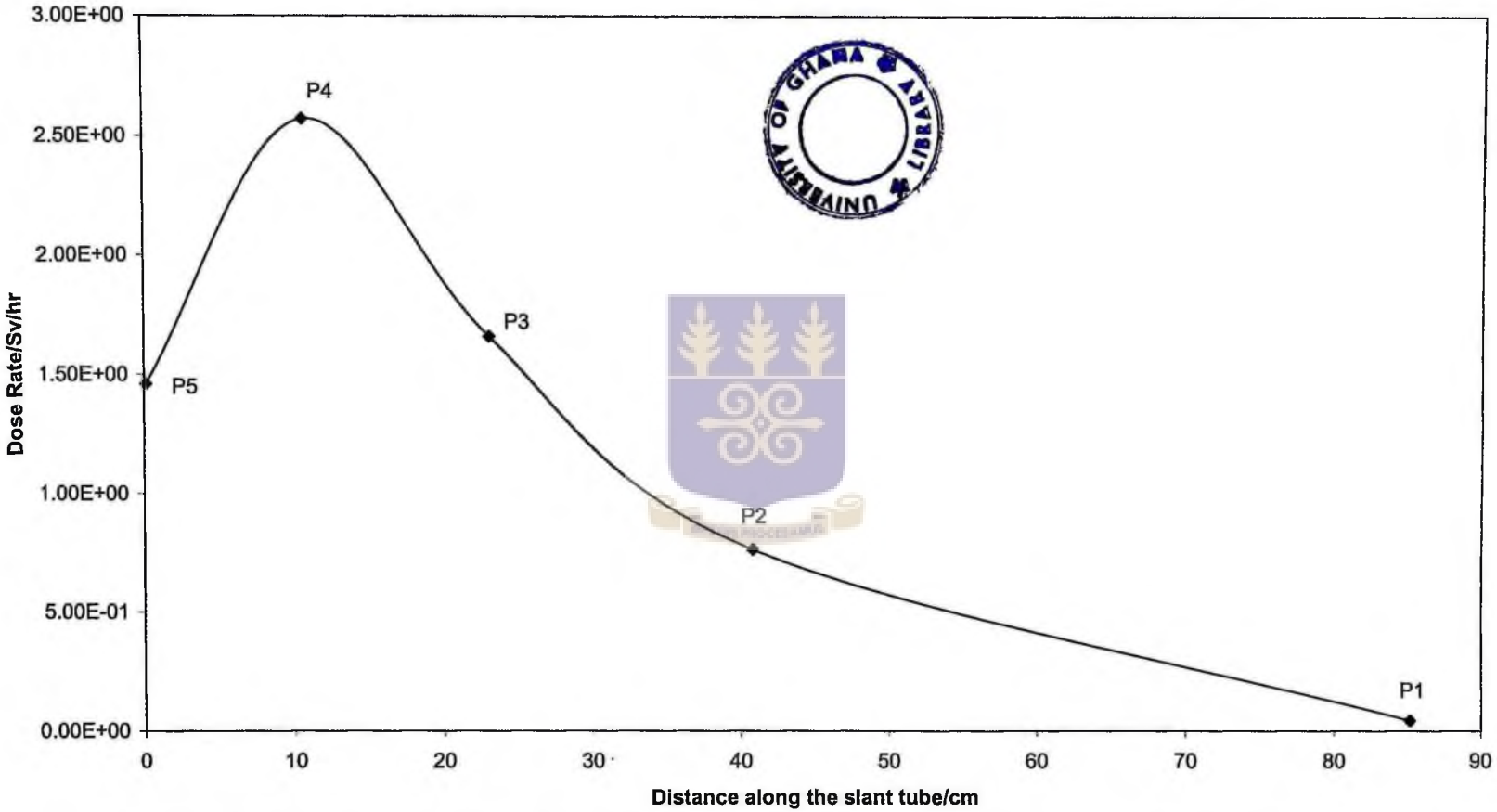

Fig. 4.93 Variation of Gamma Dose Rates at the P positions with distance along the slant tube.

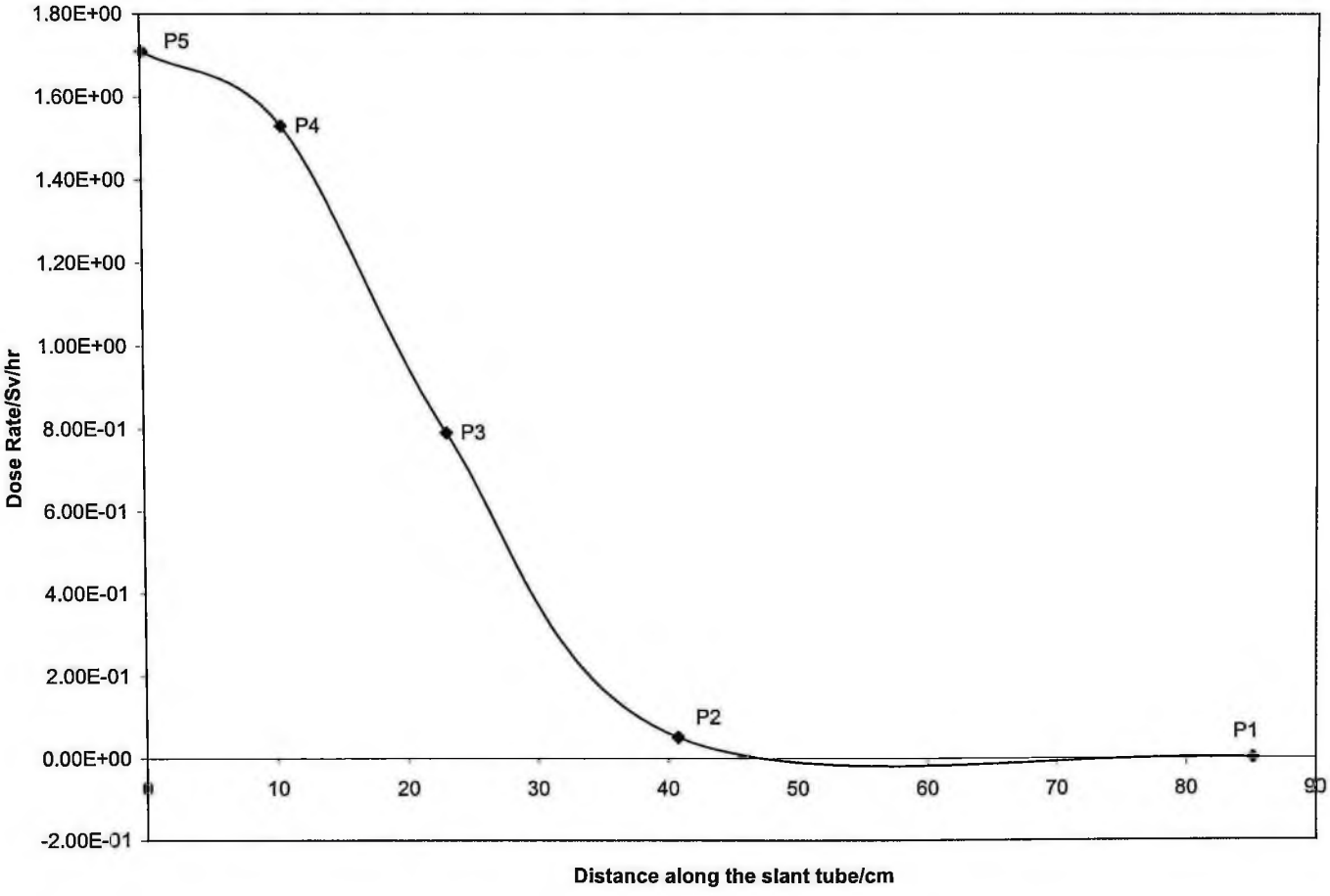

Fig. 4.94 Variation of Neutron Dose Rates at the P positions with Distance along the slant tube.

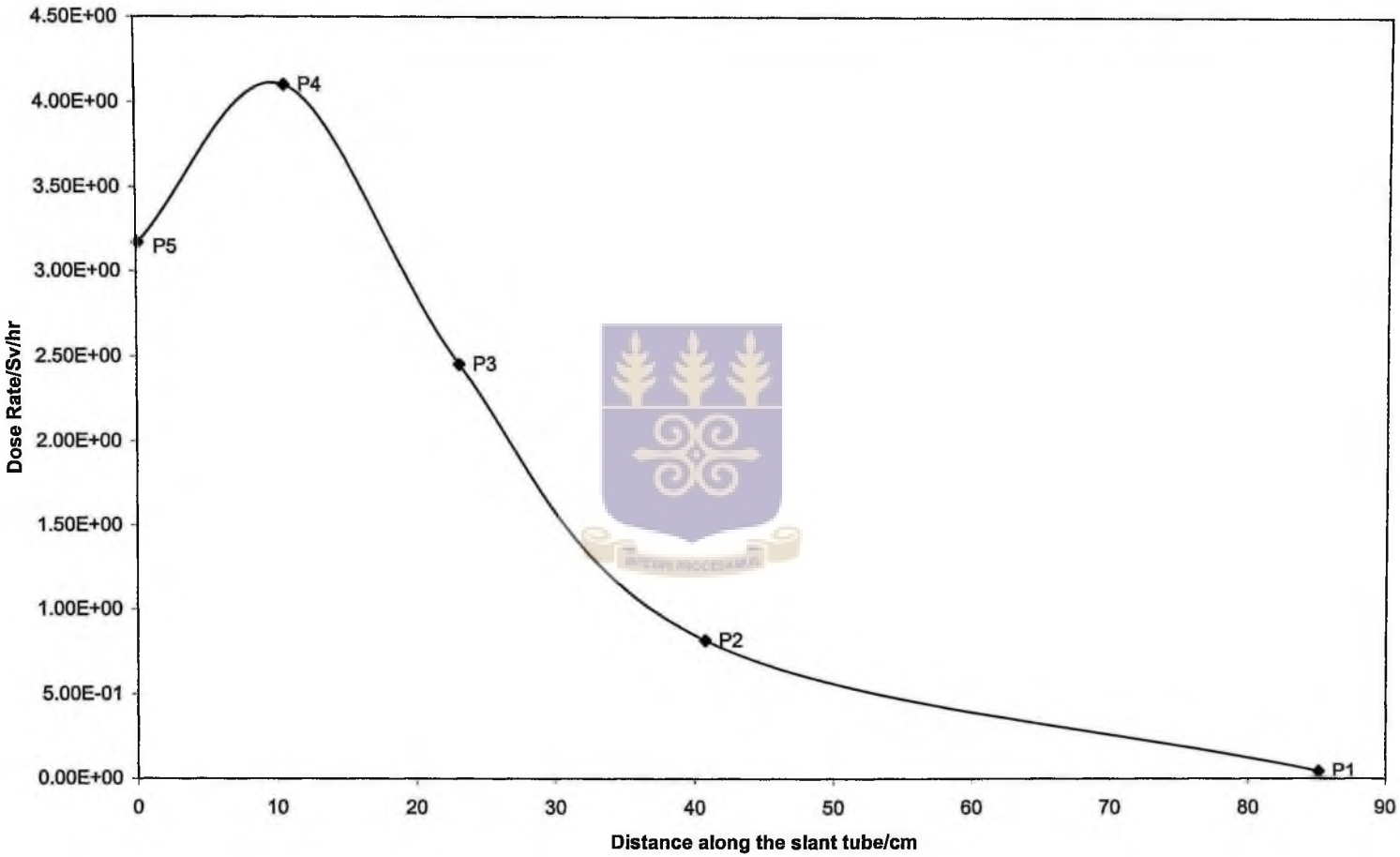

Fig. 4.95 Variation of N+G Dose Rates at the P positions with Distance along the slant tube.

CHAPTER 5

ESTIMATION OF NEUTRON AND GAMMA DOSE RATES FOR LOSS-OF-COOLANT ACCIDENTS

Two credible accidents of loss-of-coolant reported in the Safety Analysis Report of GHARR-1[7], are loss of reactor coolant and loss of pool water. An assessment of the effectiveness of the shields during these loss-of-coolant accidents is necessary for the reactor. For the analysis of these accidents, the initial condition is that the reactor vessel containing water of $1.2m^3$ in a pool water inventory of $2.7m^3$ should be operating at its maximum power of 30kW when the accidents will occur. It is also assumed that the reactor is using a fresh core with no fission products and it contains no beryllium plates in its tray located at top of the core.

Furthermore, the assumption for the loss of reactor coolant accident is that there occurs a break on the main pipe at the discharge point of the pump of the purification system. Such a loss of substantial quantity of water in the reactor vessel would be detected by the operators from the low level alarm signal and γ – radiation monitoring system installed on the control console and microcomputer control system. In case the operators failed to notice its occurrence there will be at least 500cm thickness of water above the core because the location of the lowest position of the inlet pipe of the purification system is 500cm above the core.

The loss of pool water shielding is only possible due to the maximum credible accident caused by a major earth movement; breaking of the pool and allowing the pool water to drain. It is not credible that there could be simultaneous loss of reactor vessel water due to the fact that the container was designed to support its contents while suspended within the empty pool.

An assessment of the effectiveness of the shields during these loss-of-coolants accidents is necessary for the update of the Safety Analysis Report for the reactor. The main objective of this work is to describe the theoretical analysis of these accidents and to present calculated results in order to ascertain the effectiveness of the water shield as its height is lowered in order to ascertain the radiological consequences.

In the analysis, the 1-D transport code was used to do the simulation.

Based on the satisfactory result of the validation of the calculated results of the ANISN code, it was decided to simulate postulated accidents of loss-of-coolant. The variation of dose rates for the neutron and gamma (n+g), neutron only (n), and gamma only (g) with distance are plotted in Fig. 5.1 for the reactor vessel at a depth of 200cm and for the pool depth of 240cm in Fig.5.2.

Figs. 5.3 and 5.4 show the increase of gamma dose rates with reduction of water shield in the reactor vessel and the pool respectively. It can be observed from Fig.5.3 that for the credible accident of loss of reactor vessel water, the gamma dose rates at the edge of the reactor vessel increased drastically

from 79.1 μ Sv/hr at 0cm to 246.6 μ Sv/hr at 50cm. The effect shown in Fig.5.4 is not very pronounced for the loss of pool water as compared with the accident associated with the reactor vessel.

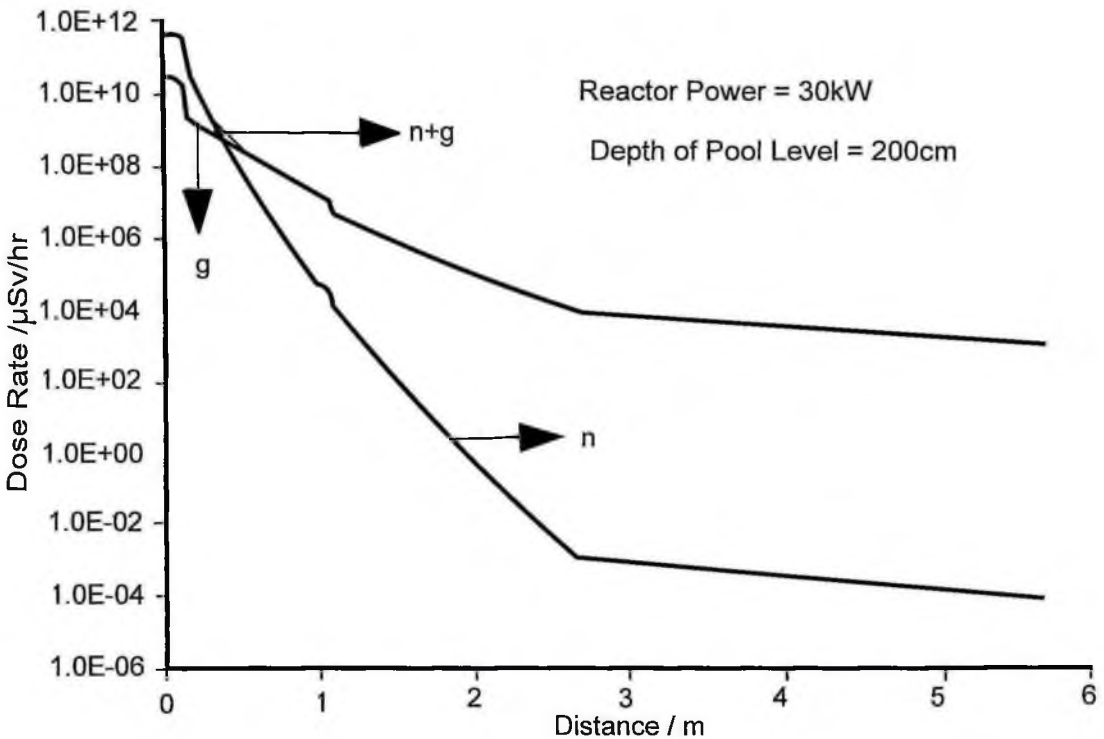

Fig: 5.1 Variation of Dose Rates with Distance for Loss Reactor Water

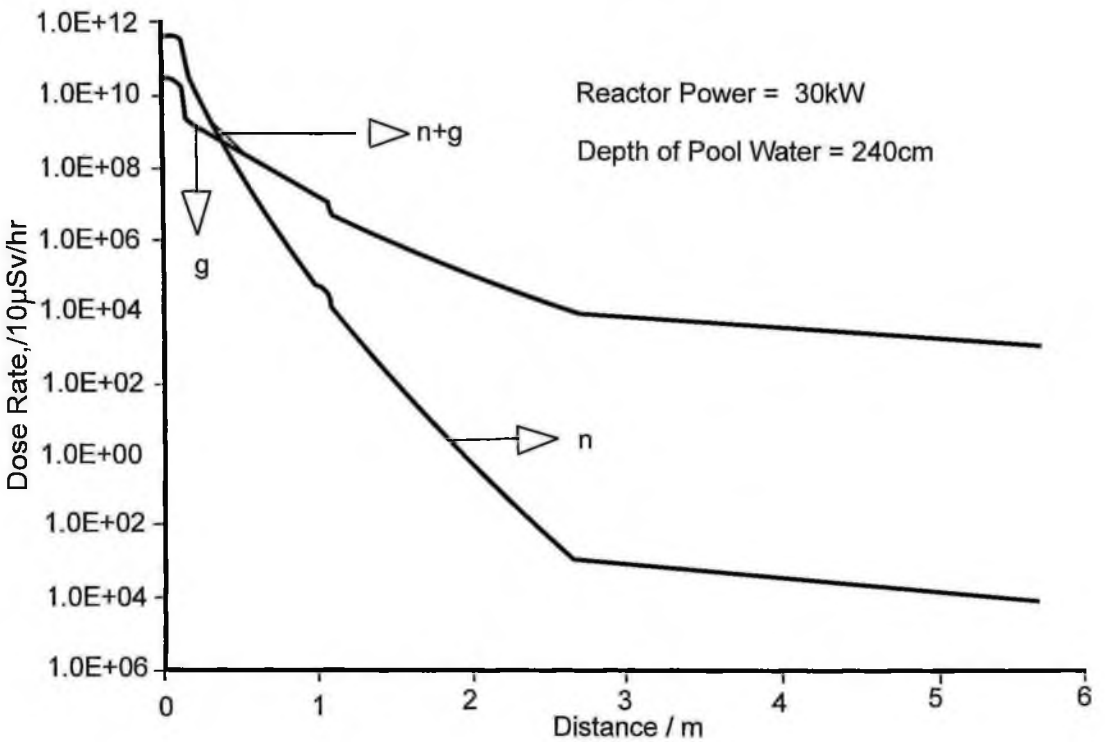

Fig:5.2 Variation of Dose Rates with Loss of Pool Water

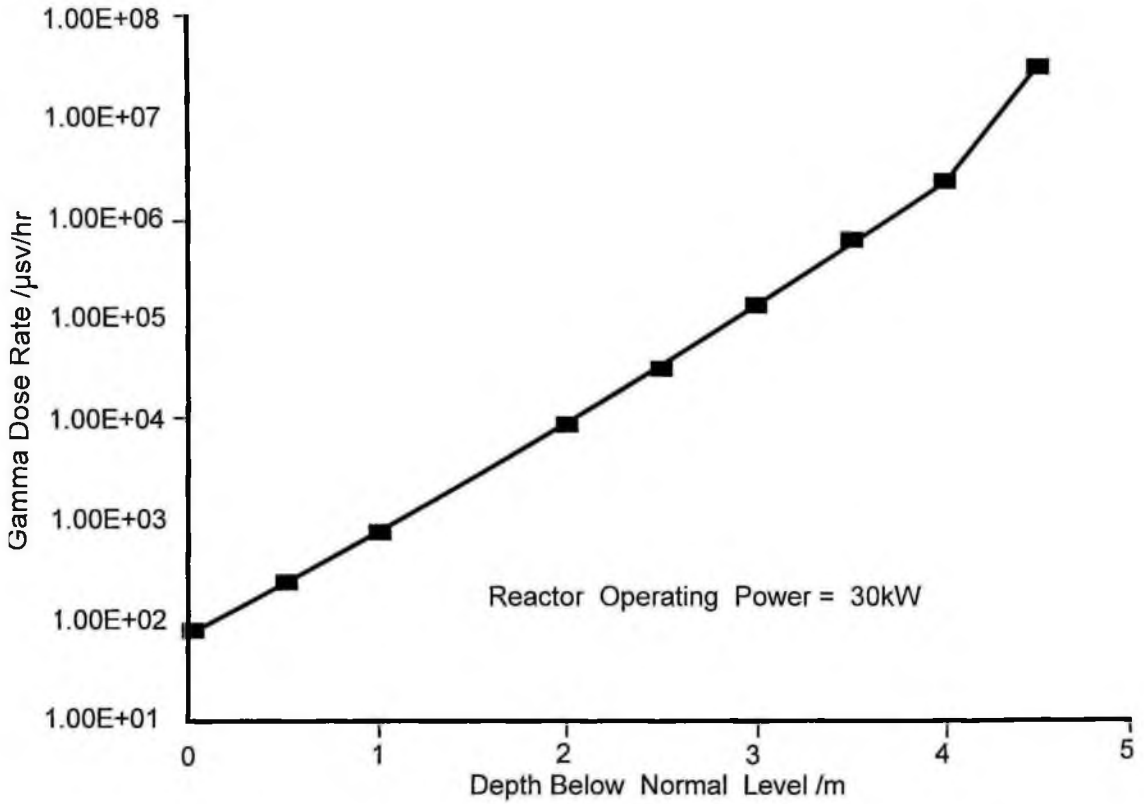

Fig: 5.3 Gamma Dose Rates with Loss of Reactor Vessel Water

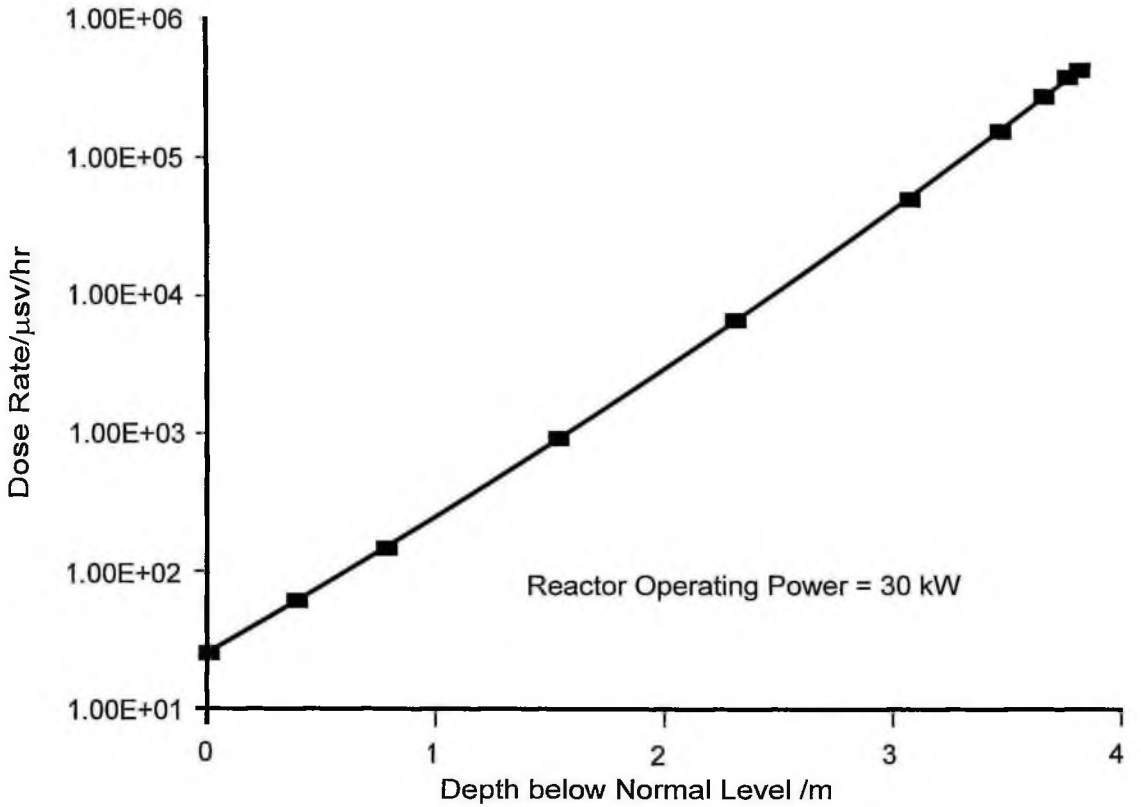

Fig:5.4 Gamma Dose Rate with Loss-of-Pool Water.

CHAPTER 6

CONCLUSIONS AND RECOMMENDATIONS

These studies present the results of the dose rates based on the solution of the 1-D transport equation solved by ANISN computer code for a tank-in-pool reactor, GHARR-1. Conclusions and recommendations that could be reached are presented as follows;

6.1 CONCLUSIONS

(a) The analyses show that the calculated results for the Gamma dose rate at different power levels agreed favourably with experimental values, with a maximum percentage variation of 8.21 with corresponding standard deviation of 0.42.

(b) The results show a drastic reduction in dose rates from the annular Be reflector through the water, the stainless steel liner and the slant tubes. This suggests the effectiveness of the water shield above the core of the reactor.

(c) Based on this satisfactory result, it was decided to study the variation of neutron (n), gamma (g) and gamma+neutron (n+g) dose rates along the slant tubes used in commissioning the reactor and to simulate postulated accidents of loss-of-coolant. The results show that;

(i) Calculations of neutron and gamma dose rates along the slant tube show decreasing levels from the bottom to the top of the slant tube. With this available information, the tube can be mapped in the future for the studies on the effect of gamma and neutron irradiation on mutation breeding of seeds in the field of agriculture.

(ii) Calculations of the effectiveness of the water shield during a loss-of-coolant in the reactor vessel and pool show significant effects of high levels of radiation. The dose rates inside the reactor hall will be high. For a break in pipe-line of the reactor vessel to the purification plant, the accident will be more severe than the case of a crack in the pool.

(iii) During a loss-of-coolant for the reactor vessel the core will not be uncovered. The consequence of the accident is likely to be less severe than that of the maximum hypothetical accidents such as collapse of the reactor building during a plane crash, fast leakage of reactor coolant and pool water or complete exposure of the core into the air.

(iv) The occurrence of a loss-of-pool water accident caused by an earthquake would result in high dose rates. Although the reactor zone is a restricted area, and no individual would be expected in the area during an accident, any staff on duty or visitor within the hall would be evacuated immediately.

6.2 RECOMMENDATIONS

(i) Apart from the instruments used in the dose measurements in this work, high dose thermolumniscent (TLD) badges could also be used as very good experimental tools to measure neutron and gamma dose rates. It is therefore recommended that measurement using a high dose TLD badges be carried out in experimental measurement of neutron and gamma dose rates at different positions along the slant tube. Measured data will be used to confirm computed results to enable the tube to be mapped for the studies on the effect of neutron and gamma irradiation on mutation breeding of seeds in the field of agriculture.

(ii) It is recommended that 2-D transport code DOT 3.5 and Monte Carlo MCNP4 for 3-D analysis be used to perform detailed shielding calculations for the reactor and all radiation emitting sources at the GHARR-1 Centre.

REFERENCES

1. J. Wood, Computational Methods in Reactor Shielding, Pergamon Press, 1982.

2. H. Cember, "Introduction to Health Physics," 2nd Ed., Pergamon Press, 1983.

3. S. Glasstone and A. Sesonske, Nuclear Reactor Engineering, Reactor Design Basics, 4th ed. Vol.1. An International Publishing Company, 1994.

4. G.F. Knoll, "Radiation Detection and Measurement," John Wiley and Sons, 1979.

5. N. Tsoulfanisdis, "Measurements and Detection of Radiation," Hemisphere Publishing Corp., 1983.

6. D.E. Cullen et al, Workshop on Reactor Physics Calculations for Applications in Nuclear Technology, World Scientific Publishing Co. Pte. Ltd. 1991.

7. E.H.K. Akaho, et al., "Ghana Research Reactor-1 Safety Analysis Report," GAEC-NNRI-RT-26, March, 1995.

8. H. Goldstein, "Fundamental Aspects of Reactor Shielding," Addison-Wesley Publishing Co., 1959.

9. W.W. Engle Jr., A users Manual for ANISN, a Dimensional Discrete Ordinates Transport Code with Anisotropic Scattering, Union Carbide Corporation, Nuclear Division, K-1693, March, 1967.

10. W.A. Rhoades and F.R. Mynatt, "The DOT-III Two-Dimensional Discrete Ordinates Transport Code," U.S.AEC Report ORNL-TM-4280, 1973.

11. M.B. Emmet, " The MORSE Monte Carlo Radiation Transport Code System," U.S. ERDA Report ORNL-4972, 1975.

12. L.M. Petrie and N.F. Cross, U.S. NRC Report NUREG/CR-0200, 1985.

13. J. Spanier and E.M. Gelbard, "Monte Carlo Principles and Neutron Transport, "Addison-Wesley Publishing Co., 1969.

14. K.D. Lathrop, "DTF-IV;A Fortran-IV program for Solving the Multigroup Transport Equation with Anisotropic Scatering, "U.S. AEC Report LA-3375, 1965.

15. E.H.K. Akaho et al., A Theoretical Investigation of Ghanaian Serpentines for Shielding Gamma Sources, G.A.E.C.- N.N.R.I-RT-6, June, 1990.

16. E. Amin et al., Neutron and Gamma Ray Total Dose Rate Determination Using ANISN, Radiation Physics Vol. 44, No. 1/2, pp, 119-123, 1994.

17. N.M. Schaeffer, Ed., "Reactor Shielding for Nuclear Engineering, " U.S. AEC Report TID-25951, 1973.

18. G.I. Bell and S. Glasstone, "Nuclear Reactor Theory," Van Nostrand Reinhold Co., 1970.

19. E.E. Lewis and W.F. Miller, Jr., "Computational Methods of Neutron Transport, "John Wiley and Sons, 1984.

20. K.D. Lathrop and B.G. Carlson, Discrete Ordinates Angular Quadrature of the Neutron Transport Equation, Los Alamos Scientific Laboratory, LA-3186, 1965.

21. Y. Yuewen et al., Reactor Complex, MNSR Document, MNSR-DC-2, China Institute of Atomic Energy, 1992.

22. M.J. Halsal, A Summary of WIMS-D/4 Input Options, AEEW-M 1327, Winfrith, England, 1980.

23. E.H.K. Akaho and B.T. Maakuu, Models and Methods of Neutronic Calculations for Ghana Research Reactor-1 Core, G.A.E.C.-N.N.R.T.-RT-35, August, 1995.

24. S. Anim-Sampong, Numerical Solution of a Two-Dimensional Multigroup Diffusion Equation for The Analysis of The Miniature Neutron Source Reactor (MNSR), MPhil Thesis, September, 1993.

25. S. Glasstone and A. Sesonke, Nuclear Reactor Engineering, Published by Van Nostrand Reinhold Company, 1963.

26. J.J. Duderstadt, and L.J. Hamilton, "Nuclear Reactor Analysis," John Wiley and Sons, Inc., 1976.

APPENDIX A

ANISN INPUT DATA PREPARATION

```
HIELDIND FOR GHARR-1 C RAD,P3, S8, 171 N, 36 G, SLANT-TUBE.
5$$
                    ID     PROBLEM ID NO.
                    ITH    0/1 = REG./ADJ.
                    ISCT   ORDER OF SCATTERING
                    ISN    QUADRATURE ORDER
                    IGE    1/2/3 = PLA/CYL/SPH
                    IBL    0/1/2/3 = NO REFL/REFL/PER/WHITE
                    IBR    RT. B.C. SAME AS LEFT B.C.,IBL
0                   IZM    NO. OF ZONES
9                   IM     NO. OF INTERVALS
                    IEVT   0/1/2/3/4/5/6=Q/K/ALPHA/C/Z/R/H
07                  IGM    NO. OF GROUPS
                    IHT    POS. OF SIGMA T
                    IHS    POS. OF SIGMA GG
13                  IHM    TABLE LENGTH
52                  MS     MIXING TABLE LENGTH
                    MCR    NO. MATLS. FROM CARDS
8                   MTP    NO. MATLS. FROM LIB TAPE
8                   MT     NO. OF MATLS.
                    IDFM   0/1=NONE/DENSITY FACTORS(21*)
                    IPVT   0/1/2=NONE/K/ALPHA
                    IQM    0/1=NONE/DIST. SOURCE
                    IPM    0/1/IM=NONE/S(MM,IPP)/S(MM,IM),I7
                    IPP    INTERVAL OF SHELL SOURCE
0                   IIM    INNER ITER. MAX.
                    ID1    0/1/2/3=NO/PRNT ND/PNCH N/BOTH
                    ID2    0/1/2=NO/X-SEC TAPE/PREV
                    ID3    0/N=NO/N ACT. BY ZONE
                    ID4    0/1=NO/N ACT. BY INT.
                    ICM    OUTER ITER. MAX.
                    IDAT1  0/1/2=NO/MIN/MAX TAPE
                    IDAT2  0/1=NO/DIFFUSION(24$)
                    IFG    0/1=NO/FEW GRP.
                    IFLU   0/1/2=BOTH/LINEAR/STEP
                    IFN    0/1/2=INPUT 2*/3*/PREV. CASE
                    IPRT   0/1 = PRINT X-SEC/DO NOT
                    IXTR   0/1=CALC/READ P-L CONSTANTS
6**
.0                   EV     EIGENVALUE GUESS
.0                   EVM    EIGENVALUE MODIFIER
.0E-4                EPS    PRECISION DESIRED
.0                   BF     BUCKLING FACTOR
.0                   DY     CYL OR PLA HEIGHT
.0                   DZ     PLANE DEPTH
.0                   DFM1   HT. FOR VOID CORR.
.0                   XNF    NORM. FACTOR
.0                   PV     IPVT=1/2   K/ALPHA
.5                   RYF    LAMBDA2 RELAXATION
.0E-4                XLAL   PT CNVRG EPS. IF .NE.0
.0                   XLAH   1-LAMBDA MAX.-SEARCH
.0                   EQL    EV CHANGE EPS.-SEARCH
```

0 XNPM NEW PARAM. MOD.-SEARCH

13$$

1	2	3	4	31	32	33	34	37	38	39	40	43	44	45	46	
5	86	87	88	115	116	117	118	121	122	123	124	127	128	129	130	
33	134	135	136	151	152	153	154	163	164	165	166	175	176	177	178	T
7**																
8.9938E+05	8.9939E+05	8.9939E+05	8.9939E+05	8.9939E+05	8.9938E+05											
8.9938E+05	8.9938E+05	8.9937E+05	8.9937E+05	8.9937E+05	8.9938E+05											
37R0.0	1.6903E+06	1.6903E+06	1.6903E+06	1.6903E+06	1.6903E+06											
1.6903E+06	1.6903E+06	1.6903E+06	1.6903E+06	1.6903E+06	1.6903E+06											
1.6903E+06	37R0.0	3.0569E+06	3.0569E+06	3.0569E+06	3.0569E+06											
3.0569E+06	3.0569E+06	3.0569E+06	3.0568E+06	3.0568E+06	3.0568E+06											
3.0568E+06	3.0568E+06	37R0.0	2.3064E+06	2.3065E+06	2.3065E+06											
2.3065E+06	2.3065E+06	2.3065E+06	2.3064E+06	2.3064E+06	2.3064E+06											
2.3064E+06	2.3064E+06	2.3064E+06	37R0.0	3.0232E+06	3.0232E+06											
3.0232E+06	3.0232E+06	3.0232E+06	3.0232E+06	3.0232E+06	3.0232E+06											
3.0232E+06	3.0231E+06	3.0231E+06	3.0232E+06	37R0.0	3.9404E+06											
3.9404E+06	3.9404E+06	3.9404E+06	3.9404E+06	3.9404E+06	3.9404E+06											
3.9404E+06	3.9404E+06	3.9404E+06	3.9404E+06	3.9404E+06	37R0.0											
5.0613E+06	5.0613E+06	5.0613E+06	5.0613E+06	5.0613E+06	5.0613E+06											
5.0613E+06	5.0612E+06	5.0612E+06	5.0612E+06	5.0612E+06	5.0612E+06											
37R0.0	1.4745E+07	1.4745E+07	1.4745E+07	1.4745E+07	1.4745E+07											
1.4745E+07	1.4745E+07	1.4745E+07	1.4745E+07	1.4745E+07	1.4745E+07											
1.4745E+07	37R0.0	2.3377E+07	2.3378E+07	2.3378E+07	2.3378E+07											
2.3378E+07	2.3377E+07	2.3377E+07	2.3377E+07	2.3377E+07	2.3377E+07											
2.3377E+07	2.3377E+07	37R0.0	3.6102E+07	3.6102E+07	3.6102E+07											
3.6102E+07	3.6102E+07	3.6102E+07	3.6102E+07	3.6102E+07	3.6102E+07											
3.6102E+07	3.6102E+07	3.6102E+07	37R0.0	5.4120E+07	5.4121E+07											
5.4121E+07	5.4121E+07	5.4121E+07	5.4121E+07	5.4120E+07	5.4120E+07											
5.4120E+07	5.4120E+07	5.4120E+07	5.4120E+07	37R0.0	7.9295E+07											
7.9296E+07	7.9296E+07	7.9296E+07	7.9296E+07	7.9296E+07	7.9295E+07											
7.9295E+07	7.9295E+07	7.9295E+07	7.9295E+07	7.9295E+07	37R0.0											
1.1337E+08	1.1337E+08	1.1337E+08	1.1337E+08	1.1337E+08	1.1337E+08											
1.1337E+08	1.1337E+08	1.1337E+08	1.1337E+08	1.1337E+08	1.1337E+08											
37R0.0	1.5822E+08	1.5822E+08	1.5822E+08	1.5822E+08	1.5822E+08											
1.5822E+08	1.5822E+08	1.5822E+08	1.5822E+08	1.5822E+08	1.5822E+08											
1.5822E+08	37R0.0	2.1614E+08	2.1615E+08	2.1615E+08	2.1615E+08											
2.1615E+08	2.1614E+08	2.1614E+08	2.1614E+08	2.1614E+08	2.1614E+08											
2.1614E+08	2.1614E+08	37R0.0	2.8926E+08	2.8926E+08	2.8926E+08											
2.8926E+08	2.8926E+08	2.8926E+08	2.8926E+08	2.8926E+08	2.8926E+08											
2.8926E+08	2.8926E+08	2.8926E+08	37R0.0	3.7960E+08	3.7960E+08											
3.7960E+08	3.7960E+08	3.7960E+08	3.7960E+08	3.7960E+08	3.7960E+08											
3.7960E+08	3.7959E+08	3.7959E+08	3.7960E+08	37R0.0	4.8893E+08											
4.8893E+08	4.8893E+08	4.8893E+08	4.8893E+08	4.8893E+08	4.8893E+08											
4.8893E+08	4.8892E+08	4.8892E+08	4.8892E+08	4.8893E+08	37R0.0											
6.1875E+08	6.1875E+08	6.1876E+08	6.1876E+08	6.1876E+08	6.1875E+08											
6.1875E+08	6.1875E+08	6.1875E+08	6.1875E+08	6.1875E+08	6.1875E+08											
37R0.0	7.7020E+08	7.7020E+08	7.7021E+08	7.7021E+08	7.7021E+08											
7.7020E+08	7.7020E+08	7.7020E+08	7.7020E+08	7.7019E+08	7.7019E+08											
7.7020E+08	37R0.0	9.4371E+08	9.4372E+08	9.4372E+08	9.4372E+08											
9.4372E+08	9.4371E+08	9.4371E+08	9.4371E+08	9.4370E+08	9.4370E+08											

4370E+08	9.4370E+08	37R0.0	3.5692E+08	3.5692E+08	3.5692E+08
5692E+08	3.5692E+08	3.5692E+08	3.5692E+08	3.5692E+08	3.5692E+08
5691E+08	3.5691E+08	3.5692E+08	37R0.0	7.8201E+08	7.8202E+08
3202E+08	7.8202E+08	7.8202E+08	7.8201E+08	7.8201E+08	7.8201E+08
3201E+08	7.8201E+08	7.8201E+08	7.8201E+08	37R0.0	1.3555E+09
3555E+09	1.3556E+09	1.3556E+09	1.3556E+09	1.3555E+09	1.3555E+09
3555E+09	1.3555E+09	1.3555E+09	1.3555E+09	1.3555E+09	37R0.0
5915E+09	1.5915E+09	1.5915E+09	1.5915E+09	1.5915E+09	1.5915E+09
5915E+09	1.5915E+09	1.5914E+09	1.5914E+09	1.5914E+09	1.5914E+09
37R0.0	1.8452E+09	1.8452E+09	1.8452E+09	1.8452E+09	1.8452E+09
3452E+09	1.8452E+09	1.8452E+09	1.8452E+09	1.8452E+09	1.8452E+09
3452E+09	37R0.0	2.1130E+09	2.1130E+09	2.1130E+09	2.1130E+09
1130E+09	2.1130E+09	2.1130E+09	2.1130E+09	2.1130E+09	2.1130E+09
1130E+09	2.1130E+09	37R0.0	2.3934E+09	2.3934E+09	2.3934E+09
3934E+09	2.3934E+09	2.3934E+09	2.3934E+09	2.3934E+09	2.3934E+09
3934E+09	2.3934E+09	2.3934E+09	37R0.0	2.6817E+09	2.6817E+09
6817E+09	2.6817E+09	2.6817E+09	2.6817E+09	2.6817E+09	2.6817E+09
6816E+09	2.6816E+09	2.6816E+09	2.6816E+09	37R0.0	2.9741E+09
9741E+09	2.9741E+09	2.9741E+09	2.9741E+09	2.9741E+09	2.9741E+09
9741E+09	2.9741E+09	2.9741E+09	2.9741E+09	2.9741E+09	37R0.0
8211E+09	6.8212E+09	6.8212E+09	6.8212E+09	6.8212E+09	6.8212E+09
8211E+09	6.8211E+09	6.8211E+09	6.8211E+09	6.8211E+09	6.8211E+09
37R0.0	7.9401E+09	7.9402E+09	7.9402E+09	7.9402E+09	7.9402E+09
9402E+09	7.9401E+09	7.9401E+09	7.9401E+09	7.9401E+09	7.9401E+09
9401E+09	37R0.0	8.9545E+09	8.9545E+09	8.9546E+09	8.9546E+09
9545E+09	8.9545E+09	8.9545E+09	8.9545E+09	8.9544E+09	8.9544E+09
9544E+09	8.9544E+09	37R0.0	4.8094E+09	4.8095E+09	4.8095E+09
8095E+09	4.8095E+09	4.8095E+09	4.8095E+09	4.8094E+09	4.8094E+09
8094E+09	4.8094E+09	4.8094E+09	37R0.0	5.0061E+09	5.0061E+09
0061E+09	5.0061E+09	5.0061E+09	5.0061E+09	5.0061E+09	5.0061E+09
0060E+09	5.0060E+09	5.0060E+09	5.0060E+09	37R0.0	5.1725E+09
1725E+09	5.1725E+09	5.1725E+09	5.1725E+09	5.1725E+09	5.1725E+09
1725E+09	5.1725E+09	5.1725E+09	5.1725E+09	5.1725E+09	37R0.0
3141E+09	5.3141E+09	5.3142E+09	5.3142E+09	5.3142E+09	5.3141E+09
3141E+09	5.3141E+09	5.3141E+09	5.3141E+09	5.3141E+09	5.3141E+09
37R0.0	5.4314E+09	5.4314E+09	5.4315E+09	5.4315E+09	5.4314E+09
4314E+09	5.4314E+09	5.4314E+09	5.4314E+09	5.4314E+09	5.4314E+09
4314E+09	37R0.0	5.5210E+09	5.5210E+09	5.5210E+09	5.5210E+09
5210E+09	5.5210E+09	5.5210E+09	5.5210E+09	5.5209E+09	5.5209E+09
5209E+09	5.5209E+09	37R0.0	3.7168E+09	3.7168E+09	3.7168E+09
7168E+09	3.7168E+09	3.7168E+09	3.7168E+09	3.7168E+09	3.7168E+09
7168E+09	3.7168E+09	3.7168E+09	37R0.0	9.3832E+08	9.3832E+08
3833E+08	9.3833E+08	9.3832E+08	9.3832E+08	9.3832E+08	9.3832E+08
3831E+08	9.3831E+08	9.3831E+08	9.3831E+08	37R0.0	9.3310E+08
3311E+08	9.3311E+08	9.3311E+08	9.3311E+08	9.3311E+08	9.3310E+08
3310E+08	9.3310E+08	9.3310E+08	9.3310E+08	9.3310E+08	37R0.0
8735E+09	1.8735E+09	1.8735E+09	1.8735E+09	1.8735E+09	1.8735E+09
8735E+09	1.8735E+09	1.8735E+09	1.8735E+09	1.8735E+09	1.8735E+09
37R0.0	3.7519E+09	3.7519E+09	3.7519E+09	3.7519E+09	3.7519E+09
7519E+09	3.7519E+09	3.7518E+09	3.7518E+09	3.7518E+09	3.7518E+09
7518E+09	37R0.0	5.6383E+09	5.6383E+09	5.6383E+09	5.6383E+09
6383E+09	5.6383E+09	5.6383E+09	5.6382E+09	5.6382E+09	5.6382E+09

5382E+09	5.6382E+09	37R0.0	5.6290E+09	5.6290E+09	5.6291E+09
5291E+09	5.6291E+09	5.6290E+09	5.6290E+09	5.6290E+09	5.6290E+09
5290E+09	5.6290E+09	5.6290E+09	37R0.0	5.6001E+09	5.6002E+09
5002E+09	5.6002E+09	5.6002E+09	5.6002E+09	5.6001E+09	5.6001E+09
5001E+09	5.6001E+09	5.6001E+09	5.6001E+09	37R0.0	5.5483E+09
5483E+09	5.5483E+09	5.5483E+09	5.5483E+09	5.5483E+09	5.5483E+09
5482E+09	5.5482E+09	5.5482E+09	5.5482E+09	5.5482E+09	37R0.0
4754E+09	5.4754E+09	5.4755E+09	5.4755E+09	5.4755E+09	5.4754E+09
4754E+09	5.4754E+09	5.4754E+09	5.4754E+09	5.4754E+09	5.4754E+09
37R0.0	5.3838E+09	5.3839E+09	5.3839E+09	5.3839E+09	5.3839E+09
3838E+09	5.3838E+09	5.3838E+09	5.3838E+09	5.3838E+09	5.3838E+09
3838E+09	37R0.0	5.2825E+09	5.2826E+09	5.2826E+09	5.2826E+09
2826E+09	5.2826E+09	5.2825E+09	5.2825E+09	5.2825E+09	5.2825E+09
2825E+09	5.2825E+09	37R0.0	5.1679E+09	5.1680E+09	5.1680E+09
1680E+09	5.1680E+09	5.1680E+09	5.1679E+09	5.1679E+09	5.1679E+09
1679E+09	5.1679E+09	5.1679E+09	37R0.0	5.0425E+09	5.0425E+09
0425E+09	5.0425E+09	5.0425E+09	5.0425E+09	5.0425E+09	5.0424E+09
0424E+09	5.0424E+09	5.0424E+09	5.0424E+09	37R0.0	4.8943E+09
8943E+09	4.8943E+09	4.8943E+09	4.8943E+09	4.8943E+09	4.8943E+09
8943E+09	4.8943E+09	4.8943E+09	4.8943E+09	4.8943E+09	37R0.0
7611E+09	4.7611E+09	4.7612E+09	4.7612E+09	4.7611E+09	4.7611E+09
7611E+09	4.7611E+09	4.7611E+09	4.7611E+09	4.7611E+09	4.7611E+09
37R0.0	4.5951E+09	4.5951E+09	4.5951E+09	4.5951E+09	4.5951E+09
5951E+09	4.5951E+09	4.5951E+09	4.5951E+09	4.5951E+09	4.5951E+09
5951E+09	37R0.0	4.4491E+09	4.4491E+09	4.4491E+09	4.4491E+09
4491E+09	4.4491E+09	4.4491E+09	4.4491E+09	4.4491E+09	4.4490E+09
4490E+09	4.4491E+09	37R0.0	4.2810E+09	4.2810E+09	4.2810E+09
2810E+09	4.2810E+09	4.2810E+09	4.2810E+09	4.2810E+09	4.2810E+09
2810E+09	4.2810E+09	4.2810E+09	37R0.0	8.0669E+09	8.0669E+09
0670E+09	8.0670E+09	8.0670E+09	8.0669E+09	8.0669E+09	8.0669E+09
0669E+09	8.0668E+09	8.0668E+09	8.0669E+09	37R0.0	3.1708E+09
1708E+09	3.1708E+09	3.1708E+09	3.1708E+09	3.1708E+09	3.1708E+09
1708E+09	3.1707E+09	3.1707E+09	3.1707E+09	3.1707E+09	37R0.0
2397E+09	4.2397E+09	4.2397E+09	4.2397E+09	4.2397E+09	4.2397E+09
2397E+09	4.2396E+09	4.2396E+09	4.2396E+09	4.2396E+09	4.2396E+09
37R0.0	3.4592E+09	3.4592E+09	3.4592E+09	3.4592E+09	3.4592E+09
4592E+09	3.4592E+09	3.4592E+09	3.4592E+09	3.4592E+09	3.4592E+09
4592E+09	37R0.0	3.2991E+09	3.2992E+09	3.2992E+09	3.2992E+09
2992E+09	3.2991E+09	3.2991E+09	3.2991E+09	3.2991E+09	3.2991E+09
2991E+09	3.2991E+09	37R0.0	3.1408E+09	3.1409E+09	3.1409E+09
1409E+09	3.1409E+09	3.1408E+09	3.1408E+09	3.1408E+09	3.1408E+09
1408E+09	3.1408E+09	3.1408E+09	37R0.0	2.9868E+09	2.9868E+09
9868E+09	2.9868E+09	2.9868E+09	2.9868E+09	2.9868E+09	2.9868E+09
9868E+09	2.9868E+09	2.9868E+09	2.9868E+09	37R0.0	2.8371E+09
8371E+09	2.8371E+09	2.8371E+09	2.8371E+09	2.8371E+09	2.8371E+09
8371E+09	2.8370E+09	2.8370E+09	2.8370E+09	2.8370E+09	37R0.0
6900E+09	2.6900E+09	2.6900E+09	2.6900E+09	2.6900E+09	2.6900E+09
6900E+09	2.6900E+09	2.6900E+09	2.6900E+09	2.6900E+09	2.6900E+09
37R0.0	2.5494E+09	2.5494E+09	2.5494E+09	2.5494E+09	2.5494E+09
5494E+09	2.5494E+09	2.5494E+09	2.5494E+09	2.5494E+09	2.5494E+09
5494E+09	37R0.0	2.4127E+09	2.4127E+09	2.4127E+09	2.4127E+09
4127E+09	2.4127E+09	2.4127E+09	2.4127E+09	2.4127E+09	2.4127E+09

4127E+09	2.4127E+09	37R0.0	2.2811E+09	2.2811E+09	2.2811E+09
2811E+09	2.2811E+09	2.2811E+09	2.2811E+09	2.2811E+09	2.2811E+09
2811E+09	2.2811E+09	2.2811E+09	37R0.0	2.1543E+09	2.1543E+09
1543E+09	2.1543E+09	2.1543E+09	2.1543E+09	2.1543E+09	2.1543E+09
1543E+09	2.1543E+09	2.1543E+09	2.1543E+09	37R0.0	2.0326E+09
0326E+09	2.0326E+09	2.0326E+09	2.0326E+09	2.0326E+09	2.0326E+09
0326E+09	2.0326E+09	2.0326E+09	2.0326E+09	2.0326E+09	37R0.0
9170E+09	1.9170E+09	1.9170E+09	1.9170E+09	1.9170E+09	1.9170E+09
9170E+09	1.9170E+09	1.9170E+09	1.9170E+09	1.9170E+09	1.9170E+09
37R0.0	3.5054E+09	3.5054E+09	3.5054E+09	3.5054E+09	3.5054E+09
5054E+09	3.5054E+09	3.5054E+09	3.5054E+09	3.5054E+09	3.5054E+09
5054E+09	37R0.0	3.1014E+09	3.1014E+09	3.1015E+09	3.1015E+09
1014E+09	3.1014E+09	3.1014E+09	3.1014E+09	3.1014E+09	3.1014E+09
1014E+09	3.1014E+09	37R0.0	1.4115E+09	1.4115E+09	1.4115E+09
4115E+09	1.4115E+09	1.4115E+09	1.4115E+09	1.4115E+09	1.4115E+09
4115E+09	1.4115E+09	1.4115E+09	37R0.0	1.3250E+09	1.3250E+09
3250E+09	1.3250E+09	1.3250E+09	1.3250E+09	1.3250E+09	1.3250E+09
3250E+09	1.3250E+09	1.3250E+09	1.3250E+09	37R0.0	2.4088E+09
4088E+09	2.4088E+09	2.4088E+09	2.4088E+09	2.4088E+09	2.4088E+09
4088E+09	2.4088E+09	2.4088E+09	2.4088E+09	2.4088E+09	37R0.0
1155E+09	2.1155E+09	2.1155E+09	2.1155E+09	2.1155E+09	2.1155E+09
1155E+09	2.1155E+09	2.1155E+09	2.1155E+09	2.1155E+09	2.1155E+09
37R0.0	2.2707E+08	2.2707E+08	2.2707E+08	2.2707E+08	2.2707E+08
2707E+08	2.2707E+08	2.2707E+08	2.2707E+08	2.2707E+08	2.2707E+08
2707E+08	37R0.0	8.4854E+07	8.4854E+07	8.4855E+07	8.4855E+07
4854E+07	8.4854E+07	8.4854E+07	8.4854E+07	8.4853E+07	8.4853E+07
4853E+07	8.4853E+07	37R0.0	1.7455E+08	1.7455E+08	1.7455E+08
7455E+08	1.7455E+08	1.7455E+08	1.7455E+08	1.7455E+08	1.7455E+08
7455E+08	1.7455E+08	1.7455E+08	37R0.0	4.7090E+08	4.7091E+08
7091E+08	4.7091E+08	4.7091E+08	4.7091E+08	4.7090E+08	4.7090E+08
7090E+08	4.7090E+08	4.7090E+08	4.7090E+08	37R0.0	8.9641E+08
9641E+08	8.9642E+08	8.9642E+08	8.9641E+08	8.9641E+08	8.9641E+08
9641E+08	8.9640E+08	8.9640E+08	8.9640E+08	8.9640E+08	37R0.0
6222E+09	1.6222E+09	1.6222E+09	1.6222E+09	1.6222E+09	1.6222E+09
6222E+09	1.6222E+09	1.6222E+09	1.6222E+09	1.6222E+09	1.6222E+09
37R0.0	7.3280E+08	7.3280E+08	7.3281E+08	7.3281E+08	7.3281E+08
3280E+08	7.3280E+08	7.3280E+08	7.3280E+08	7.3279E+08	7.3279E+08
3280E+08	37R0.0	6.8453E+08	6.8453E+08	6.8453E+08	6.8453E+08
8453E+08	6.8453E+08	6.8453E+08	6.8453E+08	6.8452E+08	6.8452E+08
8452E+08	6.8452E+08	37R0.0	6.3928E+08	6.3928E+08	6.3928E+08
3928E+08	6.3928E+08	6.3928E+08	6.3928E+08	6.3928E+08	6.3927E+08
3927E+08	6.3927E+08	6.3927E+08	37R0.0	5.9697E+08	5.9698E+08
9698E+08	5.9698E+08	5.9698E+08	5.9697E+08	5.9697E+08	5.9697E+08
9697E+08	5.9697E+08	5.9697E+08	5.9697E+08	37R0.0	5.5697E+08
5697E+08	5.5697E+08	5.5697E+08	5.5697E+08	5.5697E+08	5.5697E+08
5696E+08	5.5696E+08	5.5696E+08	5.5696E+08	5.5696E+08	37R0.0
1976E+08	5.1976E+08	5.1976E+08	5.1977E+08	5.1976E+08	5.1976E+08
1976E+08	5.1976E+08	5.1976E+08	5.1976E+08	5.1976E+08	5.1976E+08
37R0.0	4.8526E+08	4.8526E+08	4.8526E+08	4.8526E+08	4.8526E+08
8526E+08	4.8526E+08	4.8526E+08	4.8526E+08	4.8526E+08	4.8526E+08
8526E+08	37R0.0	4.5178E+08	4.5178E+08	4.5178E+08	4.5178E+08
5178E+08	4.5178E+08	4.5178E+08	4.5178E+08	4.5178E+08	4.5178E+08

5178E+08	4.5178E+08	37R0.0	4.2193E+08	4.2193E+08	4.2193E+08
2193E+08	4.2193E+08	4.2193E+08	4.2193E+08	4.2193E+08	4.2193E+08
2192E+08	4.2192E+08	4.2193E+08	37R0.0	3.9248E+08	3.9248E+08
9248E+08	3.9248E+08	3.9248E+08	3.9248E+08	3.9248E+08	3.9248E+08
9248E+08	3.9248E+08	3.9248E+08	3.9248E+08	37R0.0	3.6647E+08
6647E+08	3.6647E+08	3.6647E+08	3.6647E+08	3.6647E+08	3.6647E+08
6646E+08	3.6646E+08	3.6646E+08	3.6646E+08	3.6646E+08	37R0.0
4078E+08	3.4078E+08	3.4078E+08	3.4078E+08	3.4078E+08	3.4078E+08
4078E+08	3.4078E+08	3.4078E+08	3.4078E+08	3.4078E+08	3.4078E+08
37R0.0	3.1786E+08	3.1786E+08	3.1786E+08	3.1786E+08	3.1786E+08
1786E+08	3.1786E+08	3.1786E+08	3.1786E+08	3.1786E+08	3.1786E+08
1786E+08	37R0.0	2.9614E+08	2.9615E+08	2.9615E+08	2.9615E+08
9615E+08	2.9615E+08	2.9614E+08	2.9614E+08	2.9614E+08	2.9614E+08
9614E+08	2.9614E+08	37R0.0	2.7515E+08	2.7516E+08	2.7516E+08
7516E+08	2.7516E+08	2.7516E+08	2.7515E+08	2.7515E+08	2.7515E+08
7515E+08	2.7515E+08	2.7515E+08	37R0.0	2.5668E+08	2.5668E+08
5668E+08	2.5668E+08	2.5668E+08	2.5668E+08	2.5668E+08	2.5668E+08
5667E+08	2.5667E+08	2.5667E+08	2.5668E+08	37R0.0	5.6610E+08
6610E+08	5.6610E+08	5.6610E+08	5.6610E+08	5.6610E+08	5.6610E+08
6610E+08	5.6609E+08	5.6609E+08	5.6609E+08	5.6609E+08	37R0.0
7274E+08	4.7274E+08	4.7274E+08	4.7274E+08	4.7274E+08	4.7274E+08
7274E+08	4.7274E+08	4.7273E+08	4.7273E+08	4.7273E+08	4.7273E+08
37R0.0	1.5850E+08	1.5850E+08	1.5850E+08	1.5850E+08	1.5850E+08
5850E+08	1.5850E+08	1.5850E+08	1.5850E+08	1.5850E+08	1.5850E+08
5850E+08	37R0.0	1.1613E+08	1.1613E+08	1.1613E+08	1.1613E+08
1613E+08	1.1613E+08	1.1613E+08	1.1613E+08	1.1613E+08	1.1613E+08
1613E+08	1.1613E+08	37R0.0	2.8158E+08	2.8158E+08	2.8159E+08
8159E+08	2.8158E+08	2.8158E+08	2.8158E+08	2.8158E+08	2.8158E+08
8158E+08	2.8158E+08	2.8158E+08	37R0.0	1.6701E+08	1.6701E+08
6701E+08	1.6701E+08	1.6701E+08	1.6701E+08	1.6701E+08	1.6701E+08
6701E+08	1.6701E+08	1.6701E+08	1.6701E+08	37R0.0	3.7020E+08
7021E+08	3.7021E+08	3.7021E+08	3.7021E+08	3.7021E+08	3.7020E+08
7020E+08	3.7020E+08	3.7020E+08	3.7020E+08	3.7020E+08	37R0.0
3181E+08	1.3181E+08	1.3181E+08	1.3181E+08	1.3181E+08	1.3181E+08
3181E+08	1.3181E+08	1.3180E+08	1.3180E+08	1.3180E+08	1.3180E+08
37R0.0	1.8982E+08	1.8982E+08	1.8982E+08	1.8982E+08	1.8982E+08
8982E+08	1.8982E+08	1.8982E+08	1.8982E+08	1.8982E+08	1.8982E+08
8982E+08	37R0.0	1.5788E+08	1.5788E+08	1.5789E+08	1.5789E+08
5789E+08	1.5788E+08	1.5788E+08	1.5788E+08	1.5788E+08	1.5788E+08
5788E+08	1.5788E+08	37R0.0	1.7738E+08	1.7738E+08	1.7738E+08
7738E+08	1.7738E+08	1.7738E+08	1.7738E+08	1.7738E+08	1.7738E+08
7738E+08	1.7738E+08	1.7738E+08	37R0.0	6.3046E+07	6.3046E+07
3047E+07	6.3047E+07	6.3046E+07	6.3046E+07	6.3046E+07	6.3046E+07
3046E+07	6.3045E+07	6.3045E+07	6.3046E+07	37R0.0	8.0967E+07
0968E+07	8.0968E+07	8.0968E+07	8.0968E+07	8.0968E+07	8.0967E+07
0967E+07	8.0967E+07	8.0967E+07	8.0967E+07	8.0967E+07	37R0.0
5056E+07	3.5056E+07	3.5056E+07	3.5056E+07	3.5056E+07	3.5056E+07
5056E+07	3.5056E+07	3.5055E+07	3.5055E+07	3.5055E+07	3.5055E+07
37R0.0	2.1541E+07	2.1541E+07	2.1541E+07	2.1541E+07	2.1541E+07
1541E+07	2.1541E+07	2.1541E+07	2.1541E+07	2.1541E+07	2.1541E+07
1541E+07	37R0.0	2.8447E+07	2.8447E+07	2.8448E+07	2.8448E+07
8448E+07	2.8447E+07	2.8447E+07	2.8447E+07	2.8447E+07	2.8447E+07

3447E+07	2.8447E+07	37R0.0	1.3460E+07	1.3460E+07	1.3460E+07
3460E+07	1.3460E+07	1.3460E+07	1.3460E+07	1.3460E+07	1.3460E+07
3460E+07	1.3460E+07	1.3460E+07	37R0.0	1.2972E+07	1.2972E+07
2972E+07	1.2972E+07	1.2972E+07	1.2972E+07	1.2972E+07	1.2971E+07
2971E+07	1.2971E+07	1.2971E+07	1.2971E+07	37R0.0	3.6143E+07
6144E+07	3.6144E+07	3.6144E+07	3.6144E+07	3.6144E+07	3.6143E+07
6143E+07	3.6143E+07	3.6143E+07	3.6143E+07	3.6143E+07	37R0.0
1945E+07	5.1945E+07	5.1945E+07	5.1945E+07	5.1945E+07	5.1945E+07
1945E+07	5.1945E+07	5.1944E+07	5.1944E+07	5.1944E+07	5.1944E+07
37R0.0	7.8946E+07	7.8947E+07	7.8947E+07	7.8947E+07	7.8947E+07
8947E+07	7.8946E+07	7.8946E+07	7.8946E+07	7.8946E+07	7.8946E+07
8946E+07	37R0.0	5.4358E+07	5.4358E+07	5.4359E+07	5.4359E+07
4358E+07	5.4358E+07	5.4358E+07	5.4358E+07	5.4358E+07	5.4358E+07
4358E+07	5.4358E+07	37R0.0	3.7434E+07	3.7434E+07	3.7434E+07
7435E+07	3.7434E+07	3.7434E+07	3.7434E+07	3.7434E+07	3.7434E+07
7434E+07	3.7434E+07	3.7434E+07	37R0.0	2.5760E+07	2.5761E+07
5761E+07	2.5761E+07	2.5761E+07	2.5761E+07	2.5760E+07	2.5760E+07
5760E+07	2.5760E+07	2.5760E+07	2.5760E+07	37R0.0	1.7723E+07
7723E+07	1.7723E+07	1.7723E+07	1.7723E+07	1.7723E+07	1.7723E+07
7723E+07	1.7723E+07	1.7723E+07	1.7723E+07	1.7723E+07	37R0.0
2191E+07	1.2191E+07	1.2191E+07	1.2191E+07	1.2191E+07	1.2191E+07
2191E+07	1.2191E+07	1.2191E+07	1.2190E+07	1.2191E+07	1.2191E+07
37R0.0	5.4014E+06	5.4014E+06	5.4015E+06	5.4015E+06	5.4014E+06
.4014E+06	5.4014E+06	5.4014E+06	5.4014E+06	5.4014E+06	5.4014E+06
.4014E+06	37R0.0	2.9825E+06	2.9825E+06	2.9825E+06	2.9825E+06
.9825E+06	2.9825E+06	2.9825E+06	2.9825E+06	2.9825E+06	2.9825E+06
.9825E+06	2.9825E+06	37R0.0	2.5673E+06	2.5674E+06	2.5674E+06
.5674E+06	2.5674E+06	2.5674E+06	2.5673E+06	2.5673E+06	2.5673E+06
.5673E+06	2.5673E+06	2.5673E+06	37R0.0	2.2107E+06	2.2107E+06
.2107E+06	2.2107E+06	2.2107E+06	2.2107E+06	2.2107E+06	2.2107E+06
.2107E+06	2.2107E+06	2.2107E+06	2.2107E+06	37R0.0	9.8664E+05
.8665E+05	9.8665E+05	9.8665E+05	9.8665E+05	9.8665E+05	9.8664E+05
.8664E+05	9.8664E+05	9.8664E+05	9.8664E+05	9.8664E+05	37R0.0
.1565E+05	9.1565E+05	9.1565E+05	9.1565E+05	9.1565E+05	9.1565E+05
.1565E+05	9.1564E+05	9.1564E+05	9.1564E+05	9.1564E+05	9.1564E+05
37R0.0	1.6380E+06	1.6380E+06	1.6380E+06	1.6380E+06	1.6380E+06
.6380E+06	1.6380E+06	1.6380E+06	1.6380E+06	1.6380E+06	1.6380E+06
.6380E+06	37R0.0	1.4101E+06	1.4101E+06	1.4101E+06	1.4101E+06
.4101E+06	1.4101E+06	1.4101E+06	1.4101E+06	1.4101E+06	1.4101E+06
.4101E+06	1.4101E+06	37R0.0	2.7252E+06	2.7252E+06	2.7253E+06
.7253E+06	2.7253E+06	2.7252E+06	2.7252E+06	2.7252E+06	2.7252E+06
.7252E+06	2.7252E+06	2.7252E+06	37R0.0	1.8732E+06	1.8733E+06
.8733E+06	1.8733E+06	1.8733E+06	1.8733E+06	1.8733E+06	1.8732E+06
.8732E+06	1.8732E+06	1.8732E+06	1.8732E+06	37R0.0	1.2877E+06
.2878E+06	1.2878E+06	1.2878E+06	1.2878E+06	1.2878E+06	1.2878E+06
.2877E+06	1.2877E+06	1.2877E+06	1.2877E+06	1.2877E+06	37R0.0
.8519E+05	8.8520E+05	8.8520E+05	8.8520E+05	8.8520E+05	8.8520E+05
.8519E+05	8.8519E+05	8.8519E+05	8.8519E+05	8.8519E+05	8.8519E+05
37R0.0	6.0844E+05	6.0844E+05	6.0845E+05	6.0845E+05	6.0844E+05
.0844E+05	6.0844E+05	6.0844E+05	6.0844E+05	6.0844E+05	6.0844E+05
.0844E+05	37R0.0	4.1822E+05	4.1823E+05	4.1823E+05	4.1823E+05
.1823E+05	4.1822E+05	4.1822E+05	4.1822E+05	4.1822E+05	4.1822E+05

.822E+05	4.1822E+05	37R0.0	2.8744E+05	2.8744E+05	2.8744E+05
3744E+05	2.8744E+05	2.8744E+05	2.8744E+05	2.8744E+05	2.8744E+05
3744E+05	2.8744E+05	2.8744E+05	37R0.0	1.9760E+05	1.9760E+05
9760E+05	1.9760E+05	1.9760E+05	1.9760E+05	1.9760E+05	1.9760E+05
9760E+05	1.9760E+05	1.9760E+05	1.9760E+05	37R0.0	1.3579E+05
3579E+05	1.3579E+05	1.3579E+05	1.3579E+05	1.3579E+05	1.3579E+05
3579E+05	1.3579E+05	1.3579E+05	1.3579E+05	1.3579E+05	37R0.0
3320E+04	9.3320E+04	9.3320E+04	9.3321E+04	9.3320E+04	9.3320E+04
3320E+04	9.3319E+04	9.3319E+04	9.3319E+04	9.3319E+04	9.3319E+04
37R0.0	6.4159E+04	6.4160E+04	6.4160E+04	6.4160E+04	6.4160E+04
4159E+04	6.4159E+04	6.4159E+04	6.4159E+04	6.4159E+04	6.4159E+04
4159E+04	37R0.0	4.4086E+04	4.4086E+04	4.4087E+04	4.4087E+04
4086E+04	4.4086E+04	4.4086E+04	4.4086E+04	4.4086E+04	4.4086E+04
4086E+04	4.4086E+04	37R0.0	3.0302E+04	3.0302E+04	3.0302E+04
0302E+04	3.0302E+04	3.0302E+04	3.0302E+04	3.0302E+04	3.0302E+04
0302E+04	3.0302E+04	3.0302E+04	37R0.0	2.0827E+04	2.0827E+04
0827E+04	2.0827E+04	2.0827E+04	2.0827E+04	2.0827E+04	2.0827E+04
0827E+04	2.0827E+04	2.0827E+04	2.0827E+04	37R0.0	1.4314E+04
4314E+04	1.4314E+04	1.4314E+04	1.4314E+04	1.4314E+04	1.4314E+04
4314E+04	1.4314E+04	1.4314E+04	1.4314E+04	1.4314E+04	37R0.0
8376E+03	9.8376E+03	9.8377E+03	9.8377E+03	9.8376E+03	9.8376E+03
8376E+03	9.8375E+03	9.8375E+03	9.8375E+03	9.8375E+03	9.8375E+03
37R0.0	6.7623E+03	6.7623E+03	6.7623E+03	6.7623E+03	6.7623E+03
7623E+03	6.7623E+03	6.7622E+03	6.7622E+03	6.7622E+03	6.7622E+03
7622E+03	37R0.0	4.6473E+03	4.6473E+03	4.6473E+03	4.6473E+03
6473E+03	4.6473E+03	4.6473E+03	4.6473E+03	4.6473E+03	4.6473E+03
6473E+03	4.6473E+03	37R0.0	3.1941E+03	3.1941E+03	3.1941E+03
1941E+03	3.1941E+03	3.1941E+03	3.1941E+03	3.1941E+03	3.1941E+03
1941E+03	3.1941E+03	3.1941E+03	37R0.0	2.1947E+03	2.1947E+03
1947E+03	2.1947E+03	2.1947E+03	2.1947E+03	2.1947E+03	2.1947E+03
1947E+03	2.1947E+03	2.1947E+03	2.1947E+03	37R0.0	1.5090E+03
5090E+03	1.5090E+03	1.5090E+03	1.5090E+03	1.5090E+03	1.5090E+03
5090E+03	1.5090E+03	1.5090E+03	1.5090E+03	1.5090E+03	37R0.0
0369E+03	1.0369E+03	1.0369E+03	1.0369E+03	1.0369E+03	1.0369E+03
0369E+03	1.0369E+03	1.0369E+03	1.0369E+03	1.0369E+03	1.0369E+03
37R0.0	7.1268E+02	7.1268E+02	7.1268E+02	7.1268E+02	7.1268E+02
1268E+02	7.1268E+02	7.1267E+02	7.1267E+02	7.1267E+02	7.1267E+02
1267E+02	37R0.0	4.8983E+02	4.8984E+02	4.8984E+02	4.8984E+02
8984E+02	4.8983E+02	4.8983E+02	4.8983E+02	4.8983E+02	4.8983E+02
8983E+02	4.8983E+02	37R0.0	3.3665E+02	3.3665E+02	3.3665E+02
3665E+02	3.3665E+02	3.3665E+02	3.3665E+02	3.3665E+02	3.3665E+02
3665E+02	3.3665E+02	3.3665E+02	37R0.0	2.3139E+02	2.3139E+02
3139E+02	2.3139E+02	2.3139E+02	2.3139E+02	2.3139E+02	2.3139E+02
3139E+02	2.3139E+02	2.3139E+02	2.3139E+02	37R0.0	1.5901E+02
5901E+02	1.5901E+02	1.5901E+02	1.5901E+02	1.5901E+02	1.5901E+02
5901E+02	1.5901E+02	1.5901E+02	1.5901E+02	1.5901E+02	37R0.0
0930E+02	1.0930E+02	1.0930E+02	1.0930E+02	1.0930E+02	1.0930E+02
0930E+02	1.0930E+02	1.0930E+02	1.0930E+02	1.0930E+02	1.0930E+02
37R0.0	7.5115E+01	7.5116E+01	7.5116E+01	7.5116E+01	7.5116E+01
5116E+01	7.5115E+01	7.5115E+01	7.5115E+01	7.5115E+01	7.5115E+01
5115E+01	37R0.0	5.1623E+01	5.1623E+01	5.1624E+01	5.1624E+01
1624E+01	5.1623E+01	5.1623E+01	5.1623E+01	5.1623E+01	5.1623E+01

.1623E+01	5.1623E+01	37R0.0	3.5491E+01	3.5491E+01	3.5491E+01
.5491E+01	3.5491E+01	3.5491E+01	3.5491E+01	3.5491E+01	3.5490E+01
.5490E+01	3.5490E+01	3.5490E+01	37R0.0	2.4386E+01	2.4386E+01
.4387E+01	2.4387E+01	2.4386E+01	2.4386E+01	2.4386E+01	2.4386E+01
.4386E+01	2.4386E+01	2.4386E+01	2.4386E+01	37R0.0	1.6763E+01
.6763E+01	1.6763E+01	1.6763E+01	1.6763E+01	1.6763E+01	1.6763E+01
.6763E+01	1.6763E+01	1.6763E+01	1.6763E+01	1.6763E+01	37R0.0
.1518E+01	1.1518E+01	1.1518E+01	1.1518E+01	1.1518E+01	1.1518E+01
.1518E+01	1.1518E+01	1.1518E+01	1.1518E+01	1.1518E+01	1.1518E+01
37R0.0	2.2312E+01	2.2312E+01	2.2312E+01	2.2312E+01	2.2312E+01
.2312E+01	2.2312E+01	2.2312E+01	2.2312E+01	2.2312E+01	2.2312E+01
.2312E+01	37R0.0	3.0066E+00	3.0067E+00	3.0067E+00	3.0067E+00
.0067E+00	3.0067E+00	3.0066E+00	3.0066E+00	3.0066E+00	3.0066E+00
.0066E+00	3.0066E+00	37R0.0	1.1647E+06	1.1647E+06	1.1647E+06
.1647E+06	1.1647E+06	1.1647E+06	1.1647E+06	1.1647E+06	1.1647E+06
.1647E+06	1.1647E+06	1.1647E+06	37R0.0	1.0511E+07	1.0511E+07
.0511E+07	1.0511E+07	1.0511E+07	1.0511E+07	1.0511E+07	1.0511E+07
.0511E+07	1.0511E+07	1.0511E+07	1.0511E+07	37R0.0	9.4864E+07
.4865E+07	9.4865E+07	9.4865E+07	9.4865E+07	9.4864E+07	9.4864E+07
.4864E+07	9.4863E+07	9.4863E+07	9.4863E+07	9.4863E+07	37R0.0
.8227E+07	7.8228E+07	7.8228E+07	7.8228E+07	7.8228E+07	7.8227E+07
.8227E+07	7.8227E+07	7.8227E+07	7.8227E+07	7.8227E+07	7.8227E+07
37R0.0	1.3559E+08	1.3559E+08	1.3559E+08	1.3559E+08	1.3559E+08
.3559E+08	1.3559E+08	1.3559E+08	1.3559E+08	1.3559E+08	1.3559E+08
.3559E+08	37R0.0	2.3501E+08	2.3501E+08	2.3501E+08	2.3501E+08
.3501E+08	2.3501E+08	2.3501E+08	2.3501E+08	2.3501E+08	2.3501E+08
.3501E+08	2.3501E+08	37R0.0	4.0733E+08	4.0733E+08	4.0733E+08
.0733E+08	4.0733E+08	4.0733E+08	4.0733E+08	4.0733E+08	4.0732E+08
.0732E+08	4.0732E+08	4.0732E+08	37R0.0	7.0600E+08	7.0601E+08
.0601E+08	7.0601E+08	7.0601E+08	7.0600E+08	7.0600E+08	7.0600E+08
.0600E+08	7.0600E+08	7.0600E+08	7.0600E+08	37R0.0	1.2237E+09
.2237E+09	1.2237E+09	1.2237E+09	1.2237E+09	1.2237E+09	1.2237E+09
.2237E+09	1.2237E+09	1.2237E+09	1.2237E+09	1.2237E+09	37R0.0
.1209E+09	2.1210E+09	2.1210E+09	2.1210E+09	2.1210E+09	2.1210E+09
.1209E+09	2.1209E+09	2.1209E+09	2.1209E+09	2.1209E+09	2.1209E+09
37R0.0	3.6761E+09	3.6762E+09	3.6762E+09	3.6762E+09	3.6762E+09
.6761E+09	3.6761E+09	3.6761E+09	3.6761E+09	3.6761E+09	3.6761E+09
.6761E+09	37R0.0	6.3717E+09	6.3717E+09	6.3717E+09	6.3717E+09
.3717E+09	6.3717E+09	6.3717E+09	6.3717E+09	6.3716E+09	6.3716E+09
.3716E+09	6.3716E+09	37R0.0	1.1044E+10	1.1044E+10	1.1044E+10
.1044E+10	1.1044E+10	1.1044E+10	1.1044E+10	1.1044E+10	1.1044E+10
.1044E+10	1.1044E+10	1.1044E+10	37R0.0	1.9142E+10	1.9142E+10
.9142E+10	1.9142E+10	1.9142E+10	1.9142E+10	1.9142E+10	1.9142E+10
.9141E+10	1.9141E+10	1.9141E+10	1.9141E+10	37R0.0	3.3177E+10
.3177E+10	3.3177E+10	3.3177E+10	3.3177E+10	3.3177E+10	3.3177E+10
.3177E+10	3.3177E+10	3.3177E+10	3.3177E+10	3.3177E+10	37R0.0
.5568E+10	3.5568E+10	3.5568E+10	3.5568E+10	3.5568E+10	3.5568E+10
.5568E+10	3.5568E+10	3.5568E+10	3.5568E+10	3.5568E+10	3.5568E+10
37R0.0	2.1936E+10	2.1936E+10	2.1937E+10	2.1937E+10	2.1937E+10
.1936E+10	2.1936E+10	2.1936E+10	2.1936E+10	2.1936E+10	2.1936E+10
.1936E+10	37R0.0	2.7951E+10	2.7951E+10	2.7951E+10	2.7951E+10
.7951E+10	2.7951E+10	2.7951E+10	2.7950E+10	2.7950E+10	2.7950E+10

```
 7950E+10  2.7950E+10      37R0.0  7.1719E+10  7.1720E+10  7.1720E+10
.1720E+10  7.1720E+10  7.1719E+10  7.1719E+10  7.1719E+10  7.1719E+10
.1719E+10  7.1719E+10  7.1719E+10      37R0.0  6.6404E+10  6.6405E+10
.6405E+10  6.6405E+10  6.6405E+10  6.6404E+10  6.6404E+10  6.6404E+10
.6404E+10  6.6404E+10  6.6404E+10  6.6404E+10      37R0.0  4.6573E+10
.6573E+10  4.6573E+10  4.6573E+10  4.6573E+10  4.6573E+10  4.6573E+10
.6573E+10  4.6572E+10  4.6572E+10  4.6572E+10  4.6572E+10      37R0.0
.8616E+10  5.8617E+10  5.8617E+10  5.8617E+10  5.8617E+10  5.8617E+10
.8616E+10  5.8616E+10  5.8616E+10  5.8616E+10  5.8616E+10  5.8616E+10
   37R0.0  6.4000E+10  6.4000E+10  6.4001E+10  6.4001E+10  6.4001E+10
.4000E+10  6.4000E+10  6.4000E+10  6.4000E+10  6.4000E+10  6.4000E+10
.4000E+10      37R0.0  1.6104E+09  1.6104E+09  1.6104E+09  1.6104E+09
.6104E+09  1.6104E+09  1.6104E+09  1.6104E+09  1.6104E+09  1.6104E+09
.6104E+09  1.6104E+09      37R0.0  5.1924E+10  5.1924E+10  5.1924E+10
.1924E+10  5.1924E+10  5.1924E+10  5.1924E+10  5.1924E+10  5.1924E+10
.1923E+10  5.1924E+10  5.1924E+10      37R0.0  4.9093E+10  4.9093E+10
.9093E+10  4.9093E+10  4.9093E+10  4.9093E+10  4.9093E+10  4.9093E+10
.9093E+10  4.9093E+10  4.9093E+10  4.9093E+10      37R0.0  1.1686E+11
.1687E+11  1.1687E+11  1.1687E+11  1.1687E+11  1.1686E+11  1.1686E+11
.1686E+11  1.1686E+11  1.1686E+11  1.1686E+11  1.1686E+11      37R0.0
.4709E+11  1.4709E+11  1.4709E+11  1.4709E+11  1.4709E+11  1.4709E+11
.4709E+11  1.4709E+11  1.4708E+11  1.4708E+11  1.4708E+11  1.4708E+11
   37R0.0  8.7245E+10  8.7245E+10  8.7245E+10  8.7245E+10  8.7245E+10
.7245E+10  8.7245E+10  8.7244E+10  8.7244E+10  8.7244E+10  8.7244E+10
.7244E+10      37R0.0  9.7877E+10  9.7878E+10  9.7878E+10  9.7878E+10
.7878E+10  9.7878E+10  9.7877E+10  9.7877E+10  9.7877E+10  9.7877E+10
.7877E+10  9.7877E+10      37R0.0  5.3325E+10  5.3325E+10  5.3325E+10
.3325E+10  5.3325E+10  5.3325E+10  5.3325E+10  5.3325E+10  5.3325E+10
.3325E+10  5.3325E+10  5.3325E+10      37R0.0  3.3498E+10  3.3498E+10
.3498E+10  3.3498E+10  3.3498E+10  3.3498E+10  3.3498E+10  3.3498E+10
.3498E+10  3.3498E+10  3.3498E+10  3.3498E+10      37R0.0  3.4674E+10
.4674E+10  3.4674E+10  3.4674E+10  3.4674E+10  3.4674E+10  3.4674E+10
.4674E+10  3.4674E+10  3.4674E+10  3.4674E+10  3.4674E+10      37R0.0
.5891E+10  3.5891E+10  3.5891E+10  3.5891E+10  3.5891E+10  3.5891E+10
.5891E+10  3.5891E+10  3.5891E+10  3.5891E+10  3.5891E+10  3.5891E+10
   37R0.0  2.4625E+10  2.4625E+10  2.4625E+10  2.4625E+10  2.4625E+10
.4625E+10  2.4625E+10  2.4625E+10  2.4625E+10  2.4624E+10  2.4624E+10
.4625E+10      37R0.0  2.5198E+10  2.5198E+10  2.5198E+10  2.5198E+10
.5198E+10  2.5198E+10  2.5198E+10  2.5198E+10  2.5197E+10  2.5197E+10
.5197E+10  2.5197E+10      37R0.0                      T
  F 0.0  T
  F 0.0

 0.0    1.0    2.0    3.0    4.0    5.0    6.0    7.0    8.0    9.0
.0.0   11.0   11.5   12.0   13.0   14.0   18.0   22.0   26.0   30.0
14.0   38.0   42.0   46.0   50.0   54.0   58.0   62.0   66.0   70.0
74.0   78.0   79.0   80.0   81.0   82.0   83.0   84.0   85.0   86.0
37.0   88.0   89.0   90.0   90.5   91.0   91.5   92.0   93.0   94.0
  F 0.0
  0.0          0.0604938  0.0453704  0.0453704  0.0604938
    0.0604938  0.0453704  0.0453704  0.0604938  0.0
    0.0453704  0.0462962  0.0453704  0.0453704  0.0462962
```

```
   0.0453704  0.0         0.0453704  0.0453704  0.0453704
   0.0453704  0.0         0.0604938  0.0604938
* -0.975900  -0.9511897 -0.7867958 -0.5773503 -0.2182179
   0.2182179  0.5773503  0.7867958  0.9511897 -0.8164965
  -0.7867958 -0.5773503 -0.2182179  0.2182179  0.5773503
   0.7867958 -0.6172134 -0.5773503 -0.2182179  0.2182179
   0.5773503 -0.3086067 -0.2182179  0.2182179
$
2 1  1R 1  3R 1 16R 4 3R 1 1R 1  8R 1 2R 1  1R 1  2R 1
$
 49  53  57  61  65  69  73  77  81  85
$$
    49  50  51  52  49  50  51  52  49  50  51  52  49  50  51  52
    49  50  51  52  49  50  51  52
    53  54  55  56  53  54  55  56  53  54  55  56
    57  58  59  60  57  58  59  60
    61  62  63  64  61  62  63  64  61  62  63  64
    65  66  67  68  65  66  67  68
    69  70  71  72  69  70  71  72  69  70  71  72
    73  74  75  76  73  74  75  76  73  74  75  76  73  74  75  76
    73  74  75  76
    77  78  79  80  77  78  79  80  77  78  79  80  77  78  79  80
    77  78  79  80  77  78  79  80
    81  82  83  84  81  82  83  84
    85  86  87  88  85  86  87  88  85  86  87  88  85  86  87  88
    85  86  87  88  85  86  87  88
$$
     0   0   0   0   1   2   3   4   9  10  11  12  13  14  15  16
    21  22  23  24  37  38  39  40
     0   0   0   0   1   2   3   4  21  22  23  24
     0   0   0   0  37  38  39  40
     0   0   0   0   1   2   3   4  21  22  23  24
     0   0   0   0  37  38  39  40
     0   0   0   0   1   2   3   4  21  22  23  24
     0   0   0   0   5   6   7   8  25  26  27  28
    29  30  31  32  33  34  35  36
     0   0   0   0   1   2   3   4  17  18  19  20  21  22  23  24
    41  42  43  44  45  46  47  48
     0   0   0   0  37  38  39  40
     0   0   0   0   1   2   3   4  17  18  19  20  21  22  23  24
    41  42  43  44  45  46  47  48
2**
     4R 0.0             4R 3.8072E-02   4R 6.0196E-04   4R 6.5990E-05
     4R 1.9131E-02      4R 2.4607E-02
     4R 0.0             4R 6.6400E-02    4R 3.3472E-02
     4R 0.0             4R 6.0230E-01
     4R 0.0             4R 6.6400E-02   4R 3.347E-02
     4R 0.0             4R 6.0230E-01
     4R 0.0             4R 6.6400E-02   4R 3.347E-02
     4R 0.0             4R 5.8090E-02   4R 1.674E-02    4R 8.916E-03
     4R 1.381E-03
     4R 0.0             4R 7.3090E-05   4R 5.703E-03    4R 1.800E-03
```

```
 4R 9.970E-05      4R 4.6545E-06
 4R 0.0            4R 6.0230E-01
 4R 0.0            4R 7.3095E-05     4R 5.703E-03     4R 1.800E-03
 4R 9.970E-05      4R 4.6545E-06
10R 3
```